Michael Knap

Analytical and numerical approaches to strongly correlated manybody systems

MARSHALL PLAN SCHOLARSHIP PAPER

HARVARD
UNIVERSITY

Supervisors:

Prof. Dr. Wolfgang von der Linden

Institute of Theoretical and Computational Physics, Graz Universtiy of Technology

and

Prof. Dr. Eugene Demler

Department of Phyiscs, Harvard Univerisity

Graz, April 2012

to Sabrina

Contents

1 Introduction

The understanding of strongly correlated physical systems such as light-matter systems, ultracold atoms confined in optical lattices, high-temperature superconductors or magnetic materials opens the way for the development of new high-tech applications. These applications might be located in the field of quantum information processing, quantum optics, material sciences, energy sciences, or health sciences.

The above mentioned strongly correlated manybody systems can be mathematically described by means of quantum mechanical model Hamiltonians, which focus on the most important processes and properties of the systems. There exist different approaches to solve these problems.

In one approach the model Hamiltonians are mapped onto large scale eigenvalue problems, which have to be solved with sophisticated and demanding numerical methods. Another approach to tackle these strongly correlated many body systems is by analytical techniques. In this Marshall Plan Scholarship Paper I will compare those two approaches and demonstrate that the interplay of these two methods allows for a deeper physical insight.

In particular, this Marshall Plan Scholarship Paper consists of a collection of our recent publications and preprints. Part of the presented results are taken over from my PhD thesis [1].

The first chapter "Clustered Wigner crystal phases of cold polar molecules in ar-

rays of one-dimensional tubes" is an extended presentation of the manuscript [2], which is currently submitted to a journal. Latest details about the publication of this work can be found under arxiv.org:1112.5662 (2011). The second chapter "Nonequilibrium steady state for strongly-correlated many-body systems: variational cluster approach" is originally published in [3] and the third chapter "Extended self-energy functional approach for strongly-correlated lattice bosons in the superfluid phase" in [4].

2 Clustered Wigner crystal phases of cold polar molecules in arrays of one-dimensional tubes

Michael Knap Institute of Theoretical and Computational Physics, Graz University of Technology, 8010 Graz, Austria, and Department of Physics, Harvard University, Cambridge MA 02138, USA

Erez Berg Department of Physics, Harvard University, Cambridge MA 02138, USA

Martin Ganahl Institute of Theoretical and Computational Physics, Graz University of Technology, 8010 Graz, Austria

Eugene Demler Department of Physics, Harvard University, Cambridge MA 02138, USA

We analyze theoretically polar molecules confined in planar arrays of one dimensional tubes. In the classical limit, if the number of tubes is finite, new types of "clustered Wigner crystals" with increasingly many molecules per unit cell can be stabilized by tuning the in-plane angle between the dipolar moments and the tube direction. Quantum mechanically, these phases melt into distinct "clustered

Luttinger liquids." We map the phase diagram of the system and find that the requirements for cluster formation are reachable in current experiments. We discuss possible experimental signatures of clustered phases.

2.1 Introduction

Systems with competing long-range interactions often exhibit structures with emergent large length scales. Some examples include the formation of bubble and stripe domains in Langmuir-Blodgett films or in thin ferromagnetic layers [5,6], and the chain formation of magnetic particles in three-dimensional ferrofluids [7]. Long-range dipolar interactions in a back-gated two-dimensional electron gas (2DEG) have been predicted [8, 9] to lead to the existence of "microemulsion" phases intervening between the Fermi liquid and the Wigner crystal phase. Similar microemulsion phases may appear in 2DEGs subject to magnetic fields such that several Landau levels are occupied [10–13].

Theoretically, quantum emulsion phases are challenging to analyze since they involve structures at length scales ranging from the inter-particle distance to mesoscopic scales which are embedded in manybody systems. In contrast, the paradigms of manybody states are geared toward two particle correlations, such as paired states, magnetism and charge density wave. Experimentally, quantum emulsion phases are not easy to probe since transport measurements can only provide indirect evidence about their existence. Realizing long-range interactions with systems of cold polar molecules [14–19] can allow to explore emergent emulsion phases in a highly controllable setting. Moreover, in such systems few-body bound states [20] and trimer liquid phases [21] have been predicted.

Here, we demonstrate that the anisotropic and long-range character of dipolar interactions leads to new types of clustered crystal phases which appear at *inter-*

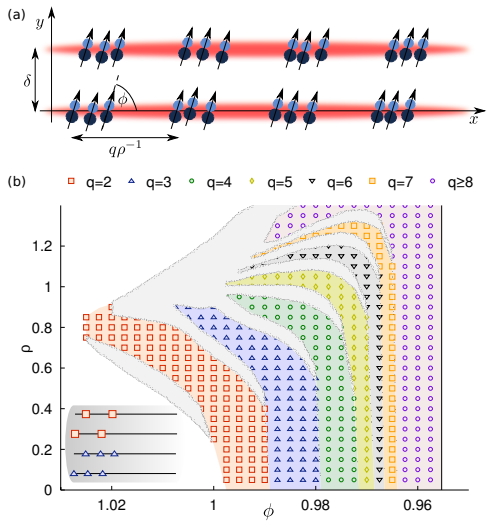

Figure 2.1: (Color online) Proposed setup to observe cluster formation of polar molecules (a). The classical phase diagram for two tubes as a function of the tilting angle ϕ and the particle density ρ is shown in (b). Lobe shaped phases consisting of clusters with q particles per tube emerge. The phase separated regions are indicated by the shaded layer surrounded with speckles. Inset: Optimized cluster configuration in one unit cell for $\phi = 1.01$, upper graph, and $\phi = 0.99$, lower graph, at $\rho = 0.7$, corresponding to $q = 2$ and $q = 3$, respectively.

mediate values of the interaction strength. Quantum mechanically, these phases melt into distinct "clustered Luttinger liquids" characterized by the decay of their density-density correlation functions. We calculate the phase diagram and study the quantum melting of the clustered phases when tuning the orientation of the dipoles. Our calculations indicate that the clustered phases can be explored under current experimental conditions.

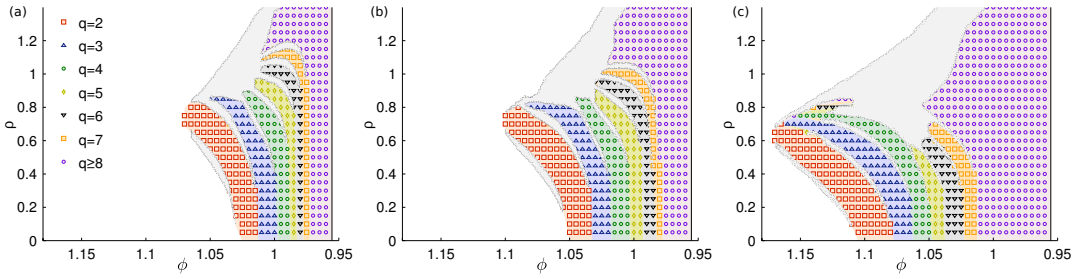

Figure 2.2: (Color online) Phase diagram in the tilting angle ϕ and the particle density ρ plane for (a) $n_T = 3$, (b) $n_T = 4$, and (c) $n_T = 8$ tubes. The phase separation regions are indicated by shaded layers surrounded by speckles.

2.2 Experimental setup

We consider a setup in which polar molecules are confined to n_T one-dimensional parallel tubes [see Fig. 2.1 (a)], which can be realized by deep optical lattices, that effectively suppress the inter-tube tunneling [22]. The dipolar moments are aligned in the plane of the tubes at an angle ϕ with respect to the tube direction. The inter-tube distance δ is used as unit of length throughout this work.

The interaction energy between two molecules with dipolar moment $\mathbf{m}$ is

$$V(r\mathbf{e}_r) = \frac{\mu^2 - 3(\mathbf{m}\mathbf{e}_r)^2}{r^3} \,, \tag{2.1}$$

where $r\mathbf{e}_r$ is the inter-molecule displacement and $\mathbf{m} = \mu(\cos\phi, \sin\phi, 0)^T$. For tilting angles below the critical angle $\phi_c = \arccos 1/\sqrt{3}$, the interaction between molecules in the same tube is attractive and the system is unstable. Thus, we focus on dipolar orientations $\pi/2 \geq \phi \geq \phi_c$ where the intra-tube interaction is repulsive. Yet, molecules in different tubes attract when their displacement along the tubes is not too large. It is precisely this interplay between attraction and repulsion which leads to the formation of clusters.

2.3 Classical limit

We first discuss the emergence of mesoscopic structures in the classical limit ($\hbar \to 0$).

When the dipoles are oriented perpendicular to the tubes ($\phi = \pi/2$) the ground state is a Wigner crystal with n_T molecules per unit cell and periodicity ρ^{-1}, where ρ is the linear density of molecules. Upon tilting the direction of the dipoles toward the critical angle ϕ_c, phases with an increasingly complex unit cell are formed, before eventually becoming unstable to collapse at $\phi = \phi_c$. In these phases, the unit cell consist of q particles per tube forming a superlattice with periodicity $q\rho^{-1}$. For example, a phase with $n_T = 2$ and $q = 3$ is illustrated schematically in Fig. 2.1 (a).

We have derived the phase diagram as a function of the tilting angle ϕ and the density ρ, by minimizing the classical ground state energy with respect to the position of the molecules, allowing for arbitrary periodic structures with up to $q = 8$ molecules per unit cell in each tube. The phase diagram for $n_T = 2$ is shown in Fig. 2.1 (b). At small densities we observe transitions to phases with monotonically increasing q when decreasing the tilt angle from $\pi/2$ toward ϕ_c. Phases of a fixed value of q have a lobe like structure, which bends with increasing density toward larger ϕ. Quite generally phases in Fig. 2.1 (b) terminate by phase separated regions, indicated by a shaded layer surrounded with speckles. The phase separated regions are determined by the Maxwell construction which is applicable when the interfacial energy is positive [8]. It is possible that phases with $q > 8$, not captured by our present calculation, are favorable in some parts of the phase diagram. In particular, this is the case very close to $\phi = \phi_c$ where we find that $q = 8$ has the lowest energy.

The origin of the cluster formation can be easily understood by considering the case $\phi = \phi_c$. Then, the intra-tube repulsion is precisely zero. In order to maximize

inter-tube attraction, it is favorable to form a single cluster with a macroscopic number of particles, corresponding to a $q \to \infty$ phase. As the angle is tuned toward ϕ_c, there must be either an infinite sequence of transitions to increasingly higher values of q, or a macroscopically phase separated region.

Next, we discuss systems with more than two tubes. Results for $n_T = 3$, 4, and 8 tubes are shown in Fig. 2.2. The phase diagrams for $n_T > 2$ have a similar lobe structure as in the $n_T = 2$ case. The main difference is that with increasing number of tubes the lobes extend to higher values of the tilting angle ϕ. Thus, clustered phases might be easier to observe in systems with a larger number of tubes. As in the $n_T = 2$ case, phase separated regions appear between some of the phases of different q.

A two-dimensional system which consists of an infinite number of tubes with dipoles aligned in the plane exhibits similar physics to the case of a finite number of tubes: the $q = 1$ Wigner crystal phase becomes locally unstable for an angle $\phi > \phi_c$. However, in this case, trial configurations with an increasing q have monotonically lower energy (we have tried structures with up to $q = 128$), indicating that the ground state may be phase separated. In the low density limit, the dipoles form infinitely long strings, which are mutually attractive, see appendix, and thus one can show that the system is unstable to macroscopic phase separation. Note that, for in-plane dipoles, the (logarithmically divergent) surface energy is is *positive*, see appendix, therefore macroscopic phase separation is possible (unlike the out-of-plane case [8]).

2.4 Quantum mechanical analysis

In quantum mechanical systems with continuous translational symmetry, true long-range crystalline order appears only in two dimensions or higher, even at

zero temperature. In one-dimensional systems, the density-density correlations decay for large distances as a power law. Nevertheless, one can expect that upon melting the clustered Wigner crystal phases by quantum fluctuations, these phases will remain distinguishable from each other by the nature of their quasi-long range correlations. We term the resulting phases "clustered Luttinger liquids."

In a clustered Luttinger liquid phase, the slowest-decaying component of the density-density correlations has a spatial period of $\lambda = q\rho^{-1}$. In a bosonized description, the fundamental harmonic of the density operator is therefore of the form $\cos[2\pi(x + x_0)\rho/q]$, where x_0 is a uniform shift of the crystalline configuration. In terms of the "counting field" $\phi(x)$ [23] defined relative to the crystalline configuration we obtain for the bosonized density

$$\rho(x) = \rho - \frac{1}{\pi}\nabla\phi(x) + \rho\cos\left[\frac{2\pi\rho x}{q} + \frac{2\phi(x)}{q}\right] + \ldots,$$

where the dots represent higher harmonics. The factor of q^{-1} present in the cosine alters the power law with which the density correlations decays:

$$\langle\rho(x)\rho(0)\rangle = \rho^2 - \frac{K}{2\pi^2}\frac{1}{x^2} + \frac{\rho^2}{2}\cos\frac{2\pi\rho x}{q}\left(\frac{\alpha}{x}\right)^{\frac{2K}{q^2}} \quad . \tag{2.2}$$

Here, K is the Luttinger parameter. Microscopic considerations, see appendix, suggest that $K \propto q$. Therefore, the exponent with which the density-density correlation function decays is proportional to $1/q$. Phases with larger q thus have a slower decay of the density-density correlation function, and are increasingly "classical" in nature.

In order to make quantitative predictions about the phase diagram in the presence of quantum fluctuations, we have investigated a system of two tubes numerically by means of density matrix renormalization group (DMRG) [24, 25] simula-

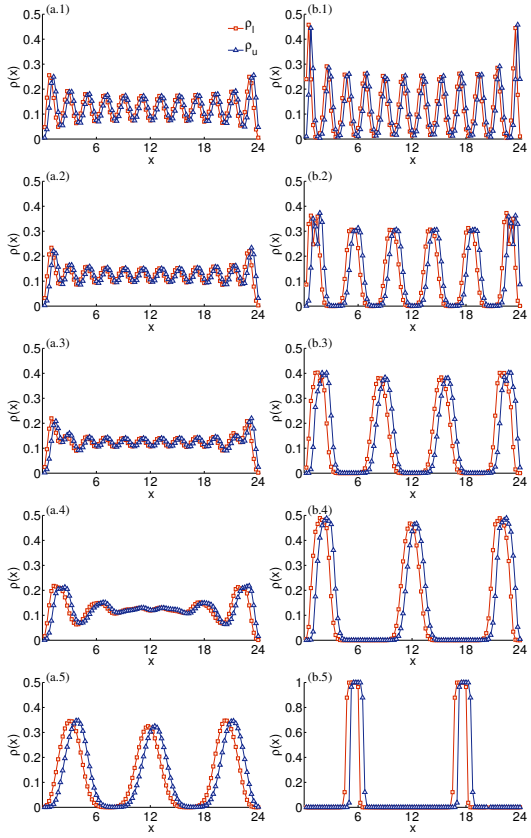

Figure 2.3: (Color online) Particle density $\rho(x)$ in the lower (red squares) and the upper (blue triangles) tube for dipolar strength $\gamma = 8$, left column, and $\gamma = 50$, right column for a system of length $L = 24\delta$, density $\rho = 0.5\delta^{-1}$ and lattice spacing $a = \delta/4$. From top to bottom the tilt angle takes the values $\phi = \{1.02, 0.99, 0.98, 0.97, 0.96\}$. For $\gamma = 50$ pronounced clusters with $q = \{1, 2, 3, 4, 6\}$ are found. The data is obtained by means of DMRG for systems with open boundary conditions.

tions. To this end, we introduce the lattice Hamiltonian

$$\hat{H} = -t \sum_{\alpha,i} \left[c^\dagger_{\alpha,i} c_{\alpha,i+1} + c^\dagger_{\alpha,i+1} c_{\alpha,i} \right] + \frac{\mu^2}{\delta^3} {\sum_{i,j,\alpha,\beta}}' V_d[(i-j)a/\delta,\, \alpha - \beta] \hat{n}_{\alpha,i} \hat{n}_{\beta,j} \,, \tag{2.3}$$

where $c_{\alpha,i}$ ($c^\dagger_{\alpha,i}$) destroys (creates) a particle at site i of tube $\alpha = 1, 2$, and $\hat{n}_{\alpha,i} = c^\dagger_{\alpha,i} c_{\alpha,i}$ counts the number of particles. Due to the strong on-site repulsion we treat the particles as hard-core, and therefore for the quantities we compute here (e.g., density distributions and ground state energies), it does not matter whether the particles are bosons or fermions. The discrete Hamiltonian can represent a continuous system by taking the lattice spacing $a \to 0$ while keeping the product $ta^2 = 1/(2m)$ constant, where t is the hopping strength and m is the mass of the particles in the continuum. The primed sum indicates that the singular contribution where $i = j$ and simultaneously $\alpha = \beta$ is omitted. The dipolar energy $V_d(x, y)$ is given by Eq. (2.1) with $\mathbf{r} = (x,\, y)^T$.

It is convenient to introduce the dimensionless quantity γ, which is the ratio between the typical dipolar interaction energy E_{dip} and the typical kinetic energy E_{kin}. These energies can be estimated as $E_{dip} \sim \mu^2 \rho^3$ and $E_{kin} \sim \rho^2/m$, respectively, and thus $\gamma \sim \mu^2 \rho m$. In the limit of strong interactions, $\gamma \gg 1$, the system is expected to be essentially classical, and the phase diagram is expected to be similar to that of Fig. 2.1 with the Wigner crystalline phases replaced by clustered Luttinger liquids. Conversely, for $\gamma \ll 1$, quantum fluctuations dominate, and we expect only the $q = 1$ phase to survive.

The particle density $\rho(x)$ evaluated with DMRG for the Hamiltonian (2.3) is shown in Fig. 2.3. We consider a system of finite length $L = 24\delta$ with open boundary conditions and particle density $\rho = 0.5\delta^{-1}$. The lattice constant is $a = \delta/4$; no significant change in the results was observed when a was decreased to $\delta/6$. The ratio between the interaction energy and the kinetic energy is $\gamma = 8$ in

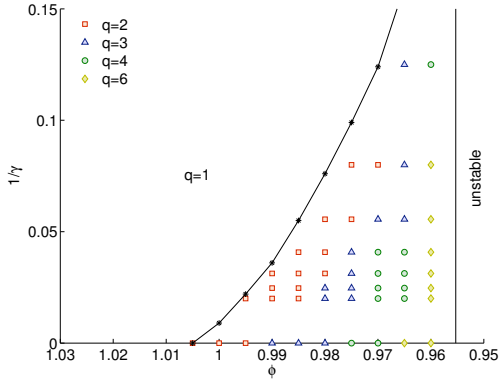

Figure 2.4: (Color online) Quantum phase diagram for a two tube system of length $L = 24\delta$, density $\rho = 0.5\delta^{-1}$, and lattice spacing $a = \delta/4$, as a function of the tilting angle ϕ and the ratio between the kinetic and the interaction energy $1/\gamma$. Right to the asterisks connected by lines cluster formation can be observed. To the left of this line, the ground state is a $q = 1$ Luttinger liquid.

Table 2.1: Numerical values for the ratio between the dipolar and the kinetic energy γ for dipoles AB and the quantities which are necessary to estimate this ratio. The dipole strength is denoted as μ and m_A (m_B) is the mass of constituent A (B). We assume the linear density to be $\rho = 10^4 \mathrm{cm}^{-1}$.

AB	μ/De	m_A/u	m_B/u	γ
KRb [26]	0.6	39.1	85.5	0.7
RbCs [27]	1.0	85.5	132.9	3.3
NaK [28]	2.7	23.0	39.1	6.8
NaCs [29]	4.6	23.0	132.9	49.4
LiCs [30]	5.5	6.9	132.9	63.3

the left and $\gamma = 50$ in the right column of the figure. For strong dipolar interactions $\gamma = 50$ we find clear signatures of clustered phases. For $\gamma = 8$ clustering of particles can be observed only for tilt angles which are very close to ϕ_c, see Fig. 2.3 (a.5). Since the reflection symmetry about a plane perpendicular to the tube is broken for any tilting angle except $\phi = \pi/2$, the density of the upper ρ_u and the lower ρ_l tube are slightly shifted. Additionally, we observe that the height of the peaks in the density decreases toward the center of the trap, consistent with quasi-long range order with density-density correlations that decay as a power law. Remarkably, the rate of the decay decreases strongly with increasing q, as expected from from the Luttinger liquid analysis, Eq. (2.2).

The complete quantum phase diagram for the two tube system as a function of the tilting angle ϕ and the ratio between the kinetic and the interaction energy $1/\gamma$ is shown in Fig. 2.4. For $1/\gamma = 0$, the results were obtained by classical minimization of the interaction energy. The DMRG simulations are used to extend the results to $1/\gamma > 0$. The phases are determined from the density distribution

by calculating the number of particles localized within one cluster. The clustered Luttinger liquid phases with $q > 1$ extent to considerably large values of $1/\gamma$, making the realization of clustered phases feasible in experiments with cold dipolar molecules.

Experimental implications.—For typical densities of $\rho = 10^4\text{cm}^{-1}$, $\gamma \sim 0.7$ can be achieved in experiments with KRb [26], $\gamma \sim 3.3$ with RbCs [27], $\gamma \sim 6.8$ with NaK [28], $\gamma \sim 49.4$ with NaCs [29], and $\gamma \sim 63.3$ with LiCs [30]. The data used to evaluate γ is summarized in Tab. 2.1.

The density regime which is most favorable for observing clustered phases is $\rho \sim 0.5\delta^{-1} - \delta^{-1}$. For $\rho \sim 10^4\text{cm}^{-1}$, this corresponds to an inter-tube separation of $\delta \sim 5 \cdot 10^{-5}\text{cm}$, easily attainable using an optical potential created by a laser with wavelength $\sim 1\mu\text{m}$.

NaCs and LiCs are thus the most promising candidates to realize clustered phases, due to their large dipolar moments. In order to make the clustered phases more robust, one can add a shallow periodic potential along the tubes. Such a periodic potential quenches the kinetic energy, thus increasing the effective value of γ. As a consequence cluster formation arises at much weaker dipolar moment also attainable by KRb.

Other effects that can be important for experiments are (i) the incommensurability of the particle number with the cluster size, (ii) the shallow trap potential along the tube direction, (iii) the strong but finite transverse confinement, (iv) quantum fluctuations in the orientation of the dipoles, and (v) finite temperature effects. Cluster formation is extremely stable with respect to (i) and (ii), see appendix. Incommensurability leads to a slight rearrangement of clusters and the consequence of the shallow trap along the tubes is merely that the distance between the clusters is reduced. One-dimensional tubes are realized by a strong transverse confinement potential (iii). Therefore, we take into account the inter-

actions computed for molecules with transverse wavefunctions, corresponding to a parabolic confinement, and compare them to the bare, one-dimensional interactions. The renormalization of the interactions due to the transverse confinement can be evaluated from a multipole expansion yielding $\Delta E^{\perp}_{\rm dip}/E_{\rm dip} \lesssim \sigma^2/\delta^2$, where we used the fact that the typical inter-molecule distance is δ and introduced σ as the spread of the wave function in transverse direction, see appendix. Under standard experimental conditions $\sigma \sim 25$nm and thus $\Delta E^{\perp}_{\rm dip}/E_{\rm dip} \lesssim 0.0025$. This ratio has to be compared with the relative energy difference between the clustered $q > 1$ and the uniform $q = 1$ phase, which typically is $0.2 - 0.5 \gg \Delta E^{\perp}_{\rm dip}/E_{\rm dip}$. Therefore, the renormalization of the interaction energy due to the finite strength of the transverse confinement is no obstacle for the observability of the clustered phases. The quantum fluctuations of the dipoles around the orientation of the electric field (iv) renormalize the dipolar potential by $\Delta E^{e}_{\rm dip}/E_{\rm dip} \lesssim R_e/\delta \sim 0.001$, where R_e is the bond length of the molecule. Thus, this effect is small as well. The temperature scale (v) below which we expect strong tendency toward cluster formation is proportional to the dipolar energy E_{dip}. In units of the Fermi temperature $T_F \sim E_{\rm kin}$ the crossover temperature is $T_{\rm cross} = \alpha\gamma$, where the proportionality constant α can be estimated from the relative energy difference of the uniform and the clustered phases, i.e., $\alpha \sim 0.2 - 0.5$. Depending on the molecule, see Tab. 2.1, the crossover temperature is $T_{\rm cross} \gtrsim T_F$.

2.5 Conclusions and Outlook

In summary, the formation of clustered phases of polar molecules is a distinct consequence of the long-range and anisotropic nature of their interactions. We find that the clustered phases can be explored under current experimental conditions. A variety of techniques can be employed to observe the clustered phases, including

elastic light scattering [31], noise correlations in time-of-flight images [32], and optical quantum nondemolition detection [20,33]. Cluster formation should also contribute additional dissociation resonances in lattice modulation experiments [34] and RF spectroscopy [35–37].

A particular exciting direction for future research is to study excitations in this system. In the case of a simple $q = 1$ crystalline phase, the unit cell consists of a single particle per tube and thus only the acoustic mode exists. However, in clustered crystal phases with $q > 1$, where the unit cell consists of more than one particle per tube, also optical branches should exist in the excitation spectra.

2.6 Appendix

2.6.1 Incommensurability and longitudinal confinement

Here, we investigate in detail the effects of the particle number incommensurability with the cluster size and of the shallow confining potential along the tube direction.

To demonstrate that the cluster formation is stable against the incommensurability of the particle number with the cluster size, we evaluate the density distribution for systems with $N = 10$, $N = 12$, and $N = 14$ polar molecules per tube, respectively. The remaining system parameters are: ratio of interaction and the kinetic energy $\gamma = 2.4$, tilt angle $\phi = 1$, length $L = 80\delta$, and lattice constant $a = \delta$. The cluster formation is commensurable with $N = 12$ particles, where four clusters with $q = 3$ particles are found, see Fig. 2.5 (b). However, both $N = 10$ and $N = 14$ are incommensurable with the $q = 3$ phase. Regardless, we observe a pronounced cluster formation, see Fig. 2.5 (a) and (c).

Next, we study the effects of the harmonic confining potential along the tube direction, which we incorporated into the Hamiltonian by a variable on-site energy $\epsilon_j = \mathcal{C}(ja - L/2)^2/L^2$. It turns out that the formation of clusters is also very

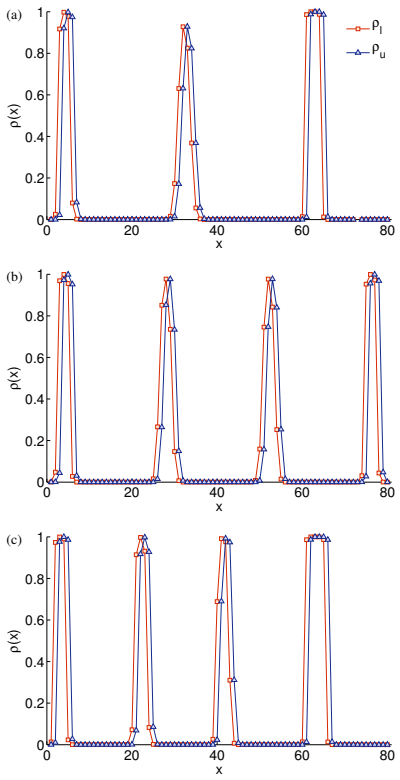

Figure 2.5: (Color online) Particle density $\rho(x)$ in the lower (red squares) and in the upper (blue triangles) tube for the ratio of the interaction to kinetic energy $\gamma = 2.4$, tilt angle $\phi = 1$, length $L = 80\delta$, and lattice constant $a = \delta$ for systems with (a) $N = 10$, (b) $N = 12$, and (c) $N = 14$ particles per tube. The cluster formation is insensitive as to particle densities which are incommensurable with the cluster size.

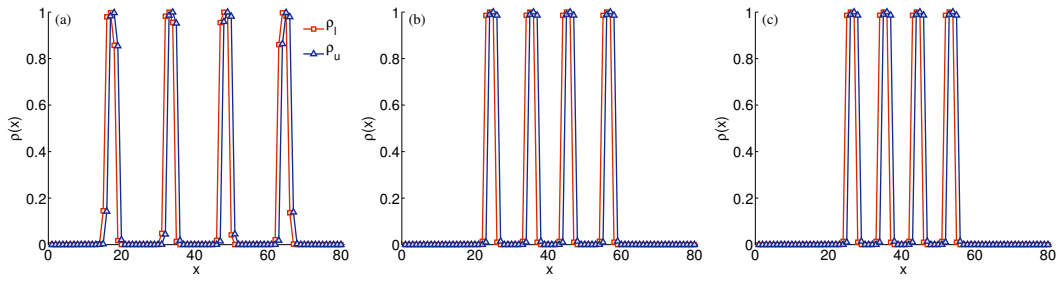

Figure 2.6: (Color online) Particle density $\rho(x)$ for the same system as described in the caption of Fig. 2.5 but with $N = 12$ throughout and a confining potential of strength (a) $\mathcal{C} = 0.1t$, (b) $\mathcal{C} = 1.0t$, and (c) $\mathcal{C} = 4.0t$. The cluster formation is robust with respect to the trap potential. The mere effect of the trap in the studied regime of the confining strength is that the distance between the clusters is reduced.

insensitive to the confining potential. Results for the particle distribution are shown in Fig. 2.6 for (a) $\mathcal{C} = 0.1t$, (b) $\mathcal{C} = 1.0t$, and (c) $\mathcal{C} = 4.0t$. For the considered values of $\mathcal{C}$, the main effect of the harmonic confinement potential is that the distance between clusters of particles is reduced as compared to the uniform case shown in Fig. 2.5 (b).

2.6.2 Multipole expansion

The renormalization of the interactions due to the fluctuations of the dipoles around the orientation of the applied electric field and due to the finite spread of the transverse wavefunctions, can be evaluated from a multipole expansion of the electric potential

$$\phi(r) = \sum_{lm} \frac{q_{lm}}{2l+1} \frac{Y_{lm}}{r^{l+1}} \,, \tag{2.4}$$

where $q_{lm} = \int Y_{lm}^* r^l \rho(\mathbf{r}) d^3\mathbf{r}$ with the charge distribution $\rho(\mathbf{r}) = \rho_+(\mathbf{r}-\mathbf{r}_e) - \rho_-(\mathbf{r}+\mathbf{r}_e)$.

The largest effect of this renormalization concerns dipoles which are separated roughly by δ. The electric field induced from one dipole at the location of the second dipole is

$$\mathbf{E}(\delta\mathbf{e}_x) = \nabla\phi(\delta\mathbf{e}_x) \ ,$$

and the potential energy is given by $V = \mathbf{mE}(\delta\mathbf{e}_x)$. The leading order term is clearly the dipole-dipole interaction $E_{22} = \mathbf{mE}_2(\delta\mathbf{e}_x)$.

The next order is the dipole-quadrupole interaction E_{42}, induced from the fluctuations of the dipoles around the electric field. This contribution is nonvanishing, since heteronuclear polar molecules are considered. From the multipole expansion (2.4) we infer the microscopic quadrupolar renormalization

$$\frac{E_{42}}{E_{22}} = \text{const.}\frac{R_e}{\delta} \ ,$$

with const. $\lesssim 1$ and R_e the bond length of the molecule.

As the transverse confinement obeys rotational symmetry, there is no quadrupole contribution from the transverse wavefunction. Therefore, the first non-vanishing contribution due to the spread of the transverse wavefunction is of the dipole-seipole (6 charges) form $E_{62} = \mathbf{mE}_6(\delta\mathbf{e}_x)$

$$\frac{E_{62}}{E_{22}} \lesssim \frac{\sigma^2}{\delta^2} \ , \tag{2.5}$$

where we used $\rho_+(\mathbf{r}) = \rho_-(\mathbf{r}) = q/(\pi\sigma^2)\exp[-(y^2+z^2)/\sigma^2]\delta(x)$ and thus $q_{lm} \sim qR_e\sigma^{l-1}$.

2.6.3 Local stability of clustered phases

One concern could be that the uniform $q = 1$ crystalline phase may be metastable, and therefore the system might not be able to find its ground state on experimental

timescales. Thus, it is useful to explicitly evaluate the stability of the uniform $q = 1$ phase. A system is locally unstable if its compressibility κ is negative. The compressibility can be evaluated from $\kappa^{-1} = \partial^2\varepsilon/\partial(\rho^{-1})^2$, where ε is the energy per particle and ρ the particle density. Thus it is useful to evaluate the spinodal line, which separates the regions with positive and negative compressibility, see asterisks connected by lines in Fig. 2.7 (a). On the right hand side of the spinodal line, close to the critical angle ϕ_c, there is a large region where the uniform $q = 1$ phase is locally unstable. In fact, it can be shown that any clustered phase (with an arbitrary q) must become locally unstable for a sufficiently large density and sufficiently close to $\phi = \phi_c$.

Assume that $\phi = \phi_c$, such that the intra-tube interaction is zero. In the high density limit, the energy per particle is proportional to the particle density times the integrated inter-tube energy. Explicitly integrating the inter-tube interaction gives $e = -\mu^2\rho\sin^2(\phi)/\delta^2$. Therefore $\kappa^{-1} < 0$. As we move away from the critical angle, the repulsive intra-tube interaction gives a contribution proportional to $(\phi - \phi_c)\rho^3$. Adding these two contributions and calculating the compressibility, we get that the critical density $\rho^\star(\phi^\star)$ at which the phase becomes unstable satisfies $\rho^\star \propto (\phi^\star - \phi_c)^{\frac{1}{2}}$.

This argument captures the main characteristics of the spinodal line at high densities. Below a certain density, the spinodal line terminates and the phase becomes locally stable, as can be seen in Fig. 2.7 (a) for $q = 1$. In Fig. 2.7 (b) we show the calculated ground state energy of the $q = 1$ phase for $\phi = 0.99$, showing the region in which $\kappa < 0$. The relative extend and shape of the spinodal line for systems with a larger but finite number of tubes, as shown in Fig. 2 in, see main text, is similar to the case of two tubes.

At the critical angle $\phi = \phi_c$ the ground state consists of dipoles which are arbitrarily close to each other corresponding to a $q = \infty$ phase. From this and

from the analysis of the compressibility follows that, there must be either an infinite sequence of phases with increasing q, or a region of macroscopic phase separation between a phase of finite q and vacuum upon approaching $\phi = \phi_c$.

2.6.4 Infinite number of tubes

Next, we study the phase diagram in the case of an infinite number of tubes. We find that the $q = 1$ phase is locally unstable in a region $\pi/2 > \phi > \phi_c$. Our results are consistent with macroscopic phase separation between the $q = 1$ phase and vacuum. So unlike the case with a finite number of tubes, intermediate phases with $q > 1$ are not realized.

The classical ground state energy of the two-dimensional system is evaluated by Ewald summation techniques [38–40]. We allow for a unit cell containing q particles. The unit cell is a parallelogram of length $q\rho^{-1}$, height δ, and an arbitrary angle. In addition, for $q > 1$, we assume that the particles within a unit cell are equally spaced. The angle and the intra-unit cell spacing are treated as variational parameters. The same scheme was used to optimize the ground state energy in the case of a finite number of tubes, and gave excellent results compared to a full optimization with respect to the positions of all the particles in the unit cell presented in, see main text [see also inset of Fig. 1 (b) in main text].

Fig. 2.8 shows the spinodal line for the $q = 1$ phase, at which the compressibility is zero. To the right of this line, the compressibility is negative, and the $q = 1$ phase is locally unstable. In the unstable regime, phases with $q > 1$ are lower in energy than the $q = 1$ phase; however, the energy decreases monotonically with increasing q, up to the largest q that we tried ($q = 128$), and is always higher than a phase separated state with macroscopic regions of $q = 1$ and vacuum. In the low density limit strings of polar molecules are formed, whose mutual interaction is attractive. Therefore, at sufficiently low densities the system always phase separates.

In two-dimensional systems with dipolar interactions, the surface tension between two phases of different density diverges logarithmically [8]. For dipoles pointing out of the plane, the divergent term is negative, and hence macroscopic phase separation is always unstable toward forming "microemulsion" phases with emergent, mesoscopic structures. For in-plane dipoles, however, the divergent energy is *positive*, and therefore macroscopic phase separation is possible.

To demonstrate this, we consider a system with a linear domain wall between two phases A and B. The dipolar contribution to the total energy is

$$E = \frac{1}{2} \int d\mathbf{r} \int d\mathbf{r}' \rho(\mathbf{r}) \rho(\mathbf{r}') V(\mathbf{r} - \mathbf{r}') \; , \tag{2.6}$$

where $\rho(\mathbf{r})$ is the density at position $\mathbf{r}$, which is ρ_A in phase A and ρ_B in phase B. Alternatively, the energy can be written as

$$E = V_A e_A + V_B e_B + E_\sigma \; , \tag{2.7}$$

where $e_A(e_B)$ is the energy density of the homogeneous $A(B)$ phase, $V_A(V_B)$ is the area of phase $A(B)$, and E_σ the surface energy between the two phases. The bulk contributions are defined as

$$V_{A(B)} e_{A(B)} = \frac{1}{2} \int_{\mathbf{r} \in \Omega_{A(B)}} d\mathbf{r} \int d\mathbf{r}' \rho_{A(B)}^2 V(\mathbf{r} - \mathbf{r}') \; ,$$

where $\Omega_{A(B)}$ defines the domain of phase $A(B)$. The integral over $\mathbf{r}'$ is taken over the entire plane $\mathbb{R}^2$. Comparing Eqs. (2.6) and (2.7) yields the surface energy

$$E_\sigma = -\frac{1}{2} \int_{\Omega_A} d\mathbf{r} \int_{\Omega_B} d\mathbf{r}' (\rho_A - \rho_B)^2 V(\mathbf{r} - \mathbf{r}') \; .$$

For dipolar interactions, E_σ / L (where L is the linear dimension of the system) diverges as $\log(L)$ as $L \to \infty$. In the following, we determine the sign of E_σ for a straight domain wall oriented along the y-direction. In order to make contact to the results of Ref. [8] where the dipoles are pointing out of plane, we consider a

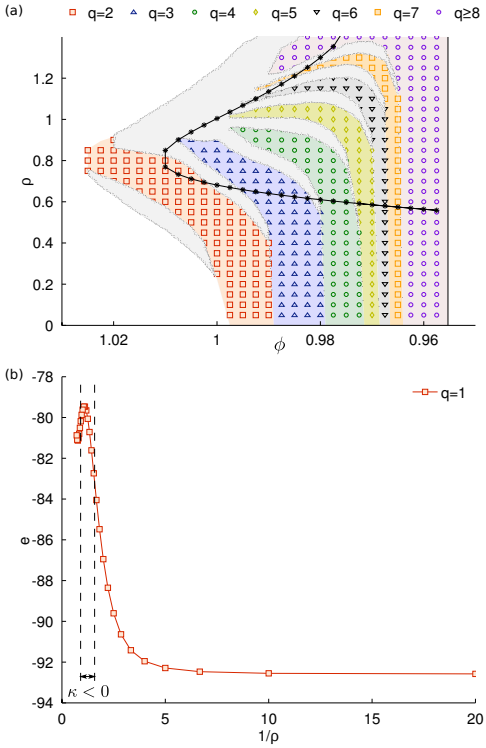

Figure 2.7: (Color online) (a) Phase diagram of dipolar molecules confined in two tubes as in Fig. 1 in the main text and spinodal line for the $q = 1$ phase, asterisks connected by lines, which separates regions of positive and negative compressibility. (b) Ground state energy of the $q = 1$ phase for $\phi = 0.99$. In the region between the dashed vertical lines the curvature of the energy per particle is negative indicating the density regime where the uniform phase is certainly unstable.

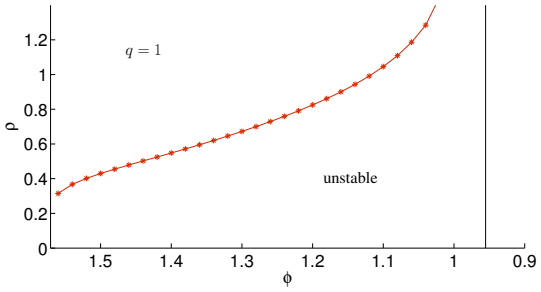

Figure 2.8: (Color online) Spinodal line for a system with infinitely many tubes, which indicates the region of instability of the $q = 1$ Wigner crystal phase.

general dipole orientation:

$$\mathbf{m} = \mu(\cos\phi\cos\theta,\ \sin\phi\cos\theta,\ \sin\theta)^T\ ,$$

where the angle θ is measured from the plane. An explicit calculation reveals that the surface energy vanishes at an angle θ_c given by

$$\theta_c = \arccos\sqrt{\frac{1}{1+\cos^2\phi}}\ .$$

For $\theta > \theta_c$, $E_\sigma < 0$, and macroscopic phase separation is impossible; for $\theta < \theta_c$, $E_\sigma > 0$ and phase separation is allowed. In particular, for $\theta = \pi/2$, $E_\sigma < 0$ (consistently with Ref. [8]), whereas for $\theta = 0$, $E_\sigma \geq 0$ for any value of ϕ.

In summary, in the case of a two-dimensional array of tubes, it seems that the $q = 1$ phase terminates at a first-order transition to vacuum, and no higher q phases exist.

Luttinger parameter K.—In order to reveal the dependence of the Luttinger parameter K of the clustered system on q, we relate it to the Luttinger parameter K_0 of the uniform ($q = 1$) system. The low-energy properties of a $q = 1$ liquid of

polar molecules in one-dimensional tubes are described by [23, 41]

$$\begin{aligned} H_{q=1} &= \int dx \rho_0 \frac{(\nabla\Theta)^2}{2m} + \frac{\mu^2\rho_0^2}{\pi^2}(\nabla\phi)^2 \\ &= \frac{u_0}{2\pi}\int dx [K_0(\nabla\Theta)^2 + \frac{1}{K_0}(\nabla\phi)^2] \,, \end{aligned}$$

where we introduced the microscopic Luttinger parameters K_0 and u_0 in the second line. The potential energy contribution is given by the particle density ρ times the dipolar energy per particle $\sim \mu^2\rho^3$. This gives in total the contribution $\sim \mu^2\rho^4$ to the energy density. Expanding the density using $\rho = \rho_0 + \delta\rho$ up to second order in $\delta\rho$ gives $\rho^4 \sim \rho_0^2\delta\rho^2 = \rho_0^2(\nabla\phi/\pi)^2$. The clustered state of polar molecules has the same kinetic energy but a reduced potential energy

$$\begin{aligned} H_q &= \int dx \rho_0 \frac{(\nabla\Theta)^2}{2m} + \frac{\mu^2\rho_0^2}{\pi^2 q^2}(\nabla\phi)^2 \\ &= \frac{u}{2\pi}\int dx [uK(\nabla\Theta)^2 + \frac{u}{K}(\nabla\phi)^2] \,, \end{aligned}$$

as the potential energy is now given by the density of clusters ρ/q times the interaction energy of a single cluster $(q\mu)^2/(q/\rho)^3$. This gives rise to the additional factor $1/q^2$. Comparing the Luttinger parameters in the $q = 1$ and $q > 1$ cases gives

$$u_0 K_0 = uK \quad \text{and} \quad \frac{1}{q^2}\frac{u_0}{K_0} = \frac{u}{K} \,,$$

leading to

$$K = qK_0 \quad \text{and} \quad u = u_0/q \,.$$

Therefore the Luttinger parameter K of the clustered Luttinger liquid is proportional to q and the decay exponent of the density-density correlation function is effectively suppressed by $1/q$, see discussion below Eq. (2) in the main text.

3 Nonequilibrium steady state for strongly-correlated many-body systems: variational cluster approach

Michael Knap Institute of Theoretical and Computational Physics, Graz University of Technology, 8010 Graz, Austria

Wolfgang von der Linden Institute of Theoretical and Computational Physics, Graz University of Technology, 8010 Graz, Austria

Enrico Arrigoni Institute of Theoretical and Computational Physics, Graz University of Technology, 8010 Graz, Austria

A numerical approach is presented that allows to compute nonequilibrium steady state properties of strongly correlated quantum many-body systems. The method is imbedded in the Keldysh Green's function formalism and is based upon the idea of the variational cluster approach as far as the treatment of strong correlations is concerned. It appears that the variational aspect is crucial as it allows for a suitable optimization of a "reference" system to the nonequilibrium target state. The approach is neither perturbative in the many-body interaction nor in the field,

that drives the system out of equilibrium, and it allows to study strong perturbations and nonlinear responses of systems in which also the correlated region is spatially extended. We apply the presented approach to non-linear transport across a strongly correlated quantum wire described by the fermionic Hubbard model.

3.1 Introduction

The theoretical understanding of the nonequilibrium behavior of strongly correlated quantum many-body systems is a long standing challenge, which has become increasingly relevant with the progress made in the fields of quantum optics and quantum simulation, semiconductor, quantum, and magnetic heterostructures, nanotechnology, or spintronics. In the field of quantum optics and quantum simulation recent advances in experiments with ultracold gases in optical lattices shed new light on strongly-correlated many body systems and their nonequilibrium properties. In these experiments, specific lattice Hamiltonians can be engineered and studied with a remarkable high level of control, making strong correlations observable on a macroscopic scale. [42–44] In this field another very promising experimental setup to study correlation effects are coupled cavity quantum electrodynamic systems which contain some form of optical nonlinearity resulting from the interaction of light with atomic levels. [45, 46] These coupled cavity systems are inherently out of equilibrium, since they are driven by external lasers and susceptible to dissipation. Semiconductor, quantum, and magnetic heterostructures subject to a bias voltage also display nonequilibrium physics, where strong correlations play a decisive role. Experiments which study transport in molecular junctions demonstrate that many-body effects, also in combination with vibrational modes are crucial, see, e.g., Refs. [47, 48]. Another class of material struc-

tures with remarkable nonequilibrium properties are (multi-well) heterostructures of diluted magnetic semiconductors (DMSs) and superlattices embedded in normal metals. These systems are of great interest as they open the possibility to tailor electronic and spintronic devices for computing and communications based on their unique interplay of spin and electronic degrees of freedom. Moreover, they display a pronounced nonlinear transport behavior. [49–55] The source of nonlinearity is also related to the strong interaction between charge carriers, excitations and vibrational modes. In addition, spin degrees of freedom clearly play a major role in their transport properties. In order to fabricate technologically useful structures the theoretical understanding of these highly correlated quantum many-body systems is indispensable.

A typical nonequilibrium situation in all these systems is conveniently described theoretically by switching on a perturbation at a certain time $\tau = \tau_0$, for example, a bias voltage, which is then kept constant after a short switching time. For this problem one may, on the one hand be interested in transient properties at short times after switching on the perturbation, for example in ultrafast pump-probe spectroscopy. [56] In this case, the properties of the system depend on the initial state, as well as on the line shape of the switch-on pulse. For longer times away from τ_0, quite generally one expects the system to reach a steady state, whose properties do not depend on details of the initial state. Nonequilibrium steady states are relevant, for example, in quantum electronic transport across heterostructures, quantum dots, molecules (see, e.g., Refs. [57–62]) or in driven-dissipative ultracold atomic systems. [63–68] Intriguingly, it was shown in Ref. [69] that nonequilibrium noise, which is present for instance in Josephson junctions, trapped ultracold polar molecules or trapped ions, still preserves the critical nonequilibrium steady states thus being a marginal perturbation as opposed to the temperature. Among the methods to treat strongly correlated systems out of equilibrium, one should

mention density-matrix renormalization group and related matrix-product state methods, [70–74] continuum-time quantum Monte-Carlo, [75] different numerical and semi-analytical renormalization-group approaches, [62, 76, 77] equation-of-motion methods, [57, 60], dynamical mean-field theory, [78–81] scattering Bethe Ansatz, [82, 83] and the dual-fermion approach. [84] Recently, Balzer and Potthoff [85] have presented a generalization of cluster-perturbation theory (CPT) to the Keldysh contour, which allows for the treatment of time-dependent phenomena. Their results show that CPT describes quite accurately the short and medium-time dynamics of a Hubbard chain. A detailed study of the short-time dynamics of weakly correlated electrons in quantum transport based on the time evolution of the nonequilibrium Kadanoff-Baym equations, where correlations are treated in Hartree-Fock-, second Born-, and GW-approximation has been given in Ref. [86]. These approximations are restricted to moderate correlations but on the other hand they allow to study rather complex models and geometries. As far as the steady-state behavior is concerned, the nonequilibrium (Keldysh) Green's function approach has been widely used on an ab-initio or tight-binding level, where correlations are treated in mean-field approximation. Since the effective particles are non-interacting, the Meir-Wingreen expression [59] for the current can be applied, which relates the current to the retarded Green's functions of the scattering with a self-energy that is renormalized due to the presence of the leads. Representative applications for nano-structured materials and molecular devices are given in Refs. [87–89] and in the review article Ref. [61].

Here we aim at strongly correlated many-body systems, and we propose a variational cluster method, that allows to study steady-state properties.

The paper is organized as follows: In Sec. 3.2 we present the variational cluster method to treat correlated systems out of equilibrium. After an introductory discussion as well as relation to previous work, we present the general method in

Sec. 3.2.1. We discuss the self-consistency condition in Sec. 3.2.2. In Sec. 3.3 we introduce two specific models describing a strongly correlated Hubbard chain and a strongly correlated Hubbard ladder, respectively, which are embedded between left and right uncorrelated reservoirs with different chemical potentials and on-site energies. This results in a voltage bias which is applied to the system. Results for the steady-state current density are discussed in Sec. 3.4. Finally, in Sec. 3.5 we present our conclusions and outlook.

3.2 Method

In order to study nonequilibrium properties of strongly correlated systems one typically considers a model consisting of two leads with uncorrelated particles, and a central correlated region. The three regions are initially decoupled. At a certain time τ_0 a coupling V between the three regions is switched on. A natural approach is to treat V via strong-coupling perturbation theory, which at the lowest order essentially corresponds to cluster-perturbation theory (CPT). In Ref. [85] it has been shown that the short time behavior can be well described within CPT. This can be understood from the observation that switching on the inter-cluster hopping V for a certain time $\Delta\tau$ produces a perturbation of order $V\,\Delta\tau$, which is accounted for at first order in CPT. Therefore, we expect the result to be accurate for small $\Delta\tau$. When addressing the steady state it is, thus, essential to improve the long-time behavior. Here, we suggest that nonequilibrium CPT can be systematically improved by minimizing some suitable "difference" between the unperturbed ("reference") state which enters CPT and the target steady state.

The strategy presented here to achieve this goal consists in exploiting the fact that the decomposition of the Hamiltonian into an "unperturbed part" and a "perturbation" is not unique. Prompted by the variational cluster approach (VCA),

one can actually add "auxiliary" single particle terms to the unperturbed Hamiltonian and subtract them again within CPT. This freedom can be exploited in order to "optimize" the results of the perturbative calculation. As discussed in detail in Refs. [90, 91], in equilibrium this is an alternative way to motivate the introduction of variational parameters in VCA. The idea discussed here, thus, provides the natural extension of VCA to treat a nonequilibrium steady state. There remains to define a criterion for the "difference" between initial and final state. (Cluster) Dynamical Mean-Field Theory [81, 92–94] (DMFT) provides a natural solution, requiring the cluster-projected Green's functions of the initial and final state to coincide. Of course, this self-consistency condition requires an infinite number of variational parameters, as well as the solution of a (cluster) impurity problem, which is computationally very expensive and whose accuracy is limited, especially in real time. In equilibrium, the self-energy functional approach [95, 96] (SFA) provides one possible generalization of DMFT if one wants to restrict to a finite number of variational parameters. In this case, the requirement for the "difference" is provided by the Euler equation (see, e.g., Eq. (7) in Ref. [95]).

In the present paper, we explore an alternative criterion, represented by (3.13), which, upon including an infinite number of bath sites, becomes equivalent to (cluster)-DMFT (see App. 3.6.1), similarly to SFA. [95] Without bath sites this corresponds to requiring that, for a given set of variational parameters $\mathbf{p}$, their conjugate operators, i.e., $dh/d\mathbf{p}$, h being the Hamiltonian, have the same expectation value in the unperturbed and in the final target state. This criterion is numerically easier to implement than the SFA, since in this case it is not necessary to search for a saddle point, which is well known to be numerically expensive. [97] In addition, inclusion of bath sites provides self consistency conditions for dynamic correlation functions as well.

The freedom discussed above can be additionally exploited by including the

hybridization between correlated regions and the leads as well as part of the leads themselves into the unperturbed Hamiltonian which is solved exactly by Lanczos exact diagonalization. In this way, CPT is then used to treat hopping terms further away from the correlated region. [98] This partly accounts for the influence of the leads onto the self-energy of the correlated region.

Finally, let us mention that the method is probably most suited to deal with models for which the correlated region is spatially extended (see Fig. 3.1). In this case, this region must be partitioned into clusters which can be solved exactly, while the intercluster terms are included into the perturbative part.

3.2.1 Variational cluster approach for nonequilibrium steady state

The physical model of interest consists of a "left" and "right" noninteracting lead, as well as a correlated region described by the Hamiltonians $\bar{h}_l$, $\bar{h}_r$, and $\bar{h}_c$, respectively, see Fig. 3.1. $\bar{h}_c$ contains local (Hubbard-type) interactions, as well as arbitrary single-particle terms. For $\tau < \tau_0$, the three regions are in equilibrium with three reservoirs at different chemical potentials, μ_l, μ_r, and μ_c respectively. The correlated region is much smaller in size than the leads, so that the latter act as relaxation baths. At $\tau = \tau_0$, the single particle (i.e., hopping) Hamiltonian terms $\hat{V}_{lc}$ and $\hat{V}_{rc}$ are switched on. These connect the left and right reservoir, respectively, with the correlated region. The total time-dependent Hamiltonian is, thus, given by

$$H(\tau) = \bar{h} + \theta(\tau - \tau_0)\hat{\bar{T}} \,, \tag{3.1}$$

where $\bar{h} = \bar{h}_c + \bar{h}_l + \bar{h}_r$, and $\hat{\bar{T}} = \hat{V}_{lc} + \hat{V}_{rc}$. We consider here the fermionic case, although many concepts can be easily extended to bosons. After a time $\Delta\tau$ long enough for relaxation to take place, the system reaches a nonequilibrium steady-

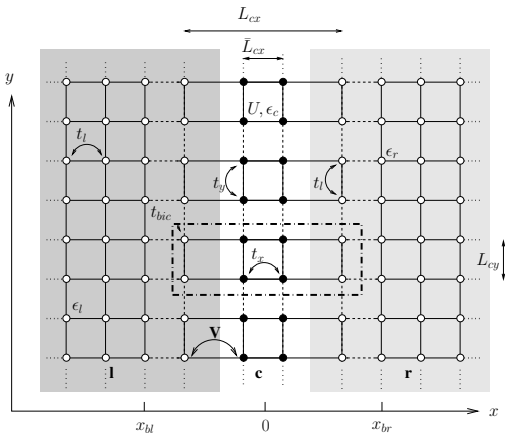

Figure 3.1: Generic scheme of the model studied here: full (empty) circles indicate correlated (uncorrelated) lattice sites. Correlated sites define the correlated region (c), and are characterized by an on-site Hubbard interaction U, an on-site energy ϵ_c, and by hopping elements t_x and t_y in the x and y direction, respectively. The physical leads (l,r), indicated by the two shaded areas, consist of half-infinite planes described by uncorrelated tight-binding models with hopping t_L, on-site energies ϵ_l and ϵ_r, and chemical potentials μ_l and μ_r, respectively. The correlated region is connected to the leads via hoppings V. The width (number of sites in the x direction) of the correlated region is $\bar{L}_{cx}$. The height of the whole system in the y direction is infinite. In this work, we study two cases, a strongly correlated chain ($\bar{L}_{cx} = 1$) and a strongly correlated two-leg ladder ($\bar{L}_{cx} = 2$), both perpendicular to the applied bias. In the variational cluster calculation the central region described by the unperturbed Hamiltonian h can differ from the physical one. The latter coincides with the correlated sites (white area in the figure). [98] On the other hand, the former consists of disconnected clusters aligned along the y direction, one of them being represented by the dash-dotted rectangle in the figure. The corresponding equilibrium Green's function is determined by Lanczos exact diagonalization.

state, with a particle current flowing from left to right for $\mu_l > \mu_r$ and from right to left for $\mu_l < \mu_r$.

As discussed above, the total $\tau > \tau_0$ Hamiltonian $H \equiv H(\tau > \tau_0)$ is decomposed into an unperturbed part h and a perturbation $\hat{T}$:

$$H = h + \hat{T} \ . \tag{3.2}$$

In the simplest CPT approach for a "small" correlated region one can take $h = \bar{h}$, and $\hat{T} = \hat{\bar{T}}$. However, when the correlated region is extended, as in Fig. 3.1, it has to be further decomposed into smaller clusters that can be solved by exact diagonalization. [99] In this case, the intercluster hopping is subtracted from h and must be included in $\hat{T}$. In addition, one can include part of the leads into the clusters (dashed lines in Fig. 3.1), so that $\hat{V}_{lc} + \hat{V}_{rc}$ are incorporated into h, while the leads intercluster hoppings (e.g. t_{bic} in the figure) are included [98] in $\hat{T}$. Finally, in the spirit of VCA, arbitrary intracluster terms Δh can be added to the unperturbed Hamiltonian and subtracted perturbatively within $\hat{T}$. In other words, calling h_{cl} the Hamiltonian describing the physical cluster partition, and $\hat{T}_{cl}$ the one describing the intercluster hoppings (dashed lines in Fig. 3.1), we write $h = h_{cl} + \Delta h$, and $\hat{T} = \hat{T}_{cl} - \Delta h$ so that the total Hamiltonian remains unchanged:

$$H = h_{cl} + \hat{T}_{cl} = h + \hat{T} \ . \tag{3.3}$$

The arbitrariness in the choice of Δh can be exploited to optimize the unperturbed state, as discussed in Ref. [91] for the equilibrium case. Here, we will adopt a different optimization criterion, see discussion below. Being a single-particle term, $\hat{T}$ is described by its hopping matrix T. This matrix has a block structure according to the three regions discussed above and shall be denoted by T_{lc}, T_{rc} and T_{cc}, respectively.

Nonequilibrium properties, in general, and nonlinear transport in particular can quite generally be determined in the frame of the Keldysh Green's function

approach. [57, 58, 100–102] Here, we adopt the notation of Ref. [58], for which the 2×2 Keldysh Green's function matrix is expressed as

$$G(\mathbf{r}, \mathbf{r}'|\tau, \tau') = \begin{pmatrix} G^R & G^K \\ 0 & G^A \end{pmatrix} , \tag{3.4}$$

where the retarded (G^R), advanced (G^A), and Keldysh (G^K) Green's functions depend in general on two lattice sites ($\mathbf{r}, \mathbf{r}'$) and two times (τ, τ'). However, both for $\tau < \tau_0$ as well as in steady state, time translation invariance holds, so that Green's functions depend only on the time difference $\tau - \tau'$, and we can Fourier transform to frequency space ω.

We use uppercase letters G to denote Green's functions of the full Hamiltonian H, and lowercase g for the ones of the unperturbed Hamiltonian h. The advantage of using the Keldysh Green's function matrix representation is that one can express Dyson's equation in the same form as in equilibrium. [57, 58] In our case, we can express it in the form

$$G = g + g\ (T + \Delta\Sigma)\ G\ , \tag{3.5}$$

where $g = \mathrm{diag}\big(g_{ll},\, g_{cc},\, g_{rr}\big)$ is block diagonal, and the products have to be considered as matrix multiplications. [103] In (3.5), $\Delta\Sigma = \Sigma - \Sigma_h$ is the difference between the (unknown) self-energy Σ of the total Hamiltonian H, including the coupling to the leads, and the self-energy Σ_h associated with the unperturbed Hamiltonian h.

The CPT approximation [104] precisely amounts to neglecting $\Delta\Sigma$. As pointed out in Ref. [85] this corresponds to neglecting irreducible diagrams containing interactions and one or more T terms. It should, however, be stressed that the self-energy of the isolated clusters is exactly included in g_{cc}, which is obtained by Lanczos exact diagonalization.

In this approximation, (3.5) can be used to obtain an equation for the Green's function G_{cc} projected onto the central region, which is still a matrix in the lattice

sites of the central region and in Keldysh space [105] (this is a straightforward generalization of, e.g., the treatment in Ref. [57]):

$$G_{cc} = g_{cc} + g_{cc}\Big(T_{cc}\, G_{cc} + \sum_{\alpha}^{\in\{l,r\}} T_{c\alpha}\, G_{\alpha c}\Big) \tag{3.6}$$

and for the lead-central region Green's functions:

$$G_{\alpha c} = g_{\alpha\alpha}\, T_{\alpha c}\, G_{cc}\,, \qquad \text{with } \alpha \in \{l, r\}. \tag{3.7}$$

It is noteworthy that Eq. (3.7) is exact and not based on the CPT approximation, as the leads contain non-interacting particles. Insertion of (3.7) into (3.6) yields

$$G_{cc} = g_{cc} + g_{cc}\big(T_{cc} + \tilde{\Sigma}_{cc}\big)\, G_{cc} \tag{3.8}$$

with the lead-induced self-energy renormalization

$$\tilde{\Sigma}_{cc} = \sum_{\alpha}^{\in\{l,r\}} T_{c\alpha}\, g_{\alpha\alpha}\, T_{\alpha c}\,. \tag{3.9}$$

Here $g_{\alpha\alpha}$ stands for the Green's function of the isolated lead α. One finally obtains a Dyson form for the steady state Green's function of the coupled system at the central region

$$G_{cc}^{-1} = g_{cc}^{-1} - T_{cc} - \tilde{\Sigma}_{cc}\,. \tag{3.10}$$

Different from the usual Dyson equation, g_{cc} is the Green's function for the isolated clusters, which contains all many-body effects inside the cluster.

For the evaluation of the current from, say, the left lead to the central region [98] one needs the G_{lc} Green's function, which is readily obtained by combining (3.7) with (3.10). This leads to the generalized Kadanoff-Baym equation (see e.g. Refs. [57,59]), along with the fact that the central region is finite in x direction and the leads are infinite, one can rewrite the current into a Büttiker-Landauer

type of formula

$$j = \int \frac{d\varepsilon}{2\pi} \big[f_F(\varepsilon - \mu_r) - f_F(\varepsilon - \mu_l) \big] \times \mathrm{Tr} \left[\; \mathrm{G}^R_{cc}\,(\varepsilon) \Gamma_l(\varepsilon) \; \mathrm{G}^A_{cc}\,(\varepsilon) \Gamma_r(\varepsilon) \right] . \tag{3.11}$$

where $G^{R/A}_{cc}$ is the retarded/advanced part of the Green's function G_{cc}, and the trace, as well as matrix products run over site indices in c. Γ_α describes the inelastic broadening owing to the coupling to lead α, which in CPT is given by [106]

$$\Gamma_\alpha = 2\,\mathrm{Im} \left\{ T_{c\alpha} g^A_{\alpha\alpha} T_{\alpha c} \right\} ,$$

which represents the contribution of lead α to the imaginary part of $\tilde{\Sigma}^A_{cc}$. Interestingly, the expression for the current in CPT has the same structure as the Meir-Wingreen formula [59] for non-interacting particles, which is the basis for nonequilibrium ab-initio-calculations. [88] Here, however, the Green's function contains the many-body interactions of the correlated region. An advantage of this expression is that it yields an explicit connection to the Green function $G^{R/A}_{cc}$ of the scattering region and the influence of the itinerant electrons in the leads. A similar expression can be derived for the one-particle density matrix between two sites with the same y coordinate, which is required for the self-consistency condition discussed below.

As it is well known, all retarded and advanced Green's functions are evaluated without chemical potentials. The latter enter through the Keldysh Green's function or rather via the Fermi functions. While the chemical potential of the central region is wiped out in the steady state due to its small size in comparison to the size of the leads, the chemical potentials of the leads explicitly enter the expressions for the current and the density matrix, see Eq. (3.11). In the case investigated here, the central region is translation invariant in y direction and is split into identical clusters. In the end, as far as the main numerical task is concerned, one has to

solve many-body problems for clusters of size $L = L_{cx} \times L_{cy}$, invert matrices of the same size, and sum over wave vectors q_y belonging to the Brillouin zone associated with the cluster supercell.

3.2.2 Self-consistency condition

Equation (3.10) is the expression for the Green's function of the central region within the CPT approximation. As discussed above, one would like to optimize the initial state in some appropriate way by suitably adjusting the parameters Δh of the unperturbed Hamiltonian h. The inclusion of additional terms Δh adds flexibility to the self-energy Σ_h which is included within this approximation. Obviously, it makes no difference in the case of non-interacting particles as the selfenergy vanishes exactly, independently of Δh. This freedom can be exploited in order to improve the approximation systematically. A similar discussion on this issue has been given in Refs. [90, 91]), and is at the basis of the VCA idea [95].

As discussed above, we need a variational condition associated with a "minimization" of the difference between unperturbed and perturbed state. In (cluster)-DMFT one requires the cluster projected Green's function to be equal to the unperturbed one

$$g_{cc} = \mathcal{P}(G_{cc}) \ , \tag{3.12}$$

where $\mathcal{P}$ projects the Green's function onto the cluster, i.e., it sets all its intercluster matrix elements to zero. [107] Since here we have a finite number of variational parameters $\mathbf{p}$ that can be adjusted, we cannot satisfy (3.12). We, thus, propose a "weaker" condition, namely that the expectation values of operators coupled to the variational parameters contained in Δh (i.e., $d\Delta h/d\mathbf{p}$) be equal in the unperturbed and in the perturbed state. More specifically, we impose the condition

$$\int \frac{d\omega}{2\pi} \operatorname{tr} \hat{\tau}_1 \frac{\partial \left(g_{0cc}\right)^{-1}}{\partial \mathbf{p}} \left(g_{cc} - G_{cc}\right) = 0 \ , \tag{3.13}$$

where $\hat{\tau}_1$ is a Pauli matrix in Keldysh space, [108] and g_{0cc} is the Green's function associated with the noninteracting part of h. It is interesting to note (see appendix 3.6.1) that by including into Δh a coupling to an infinite number of bath sites, the present method, with the self-consistence condition (3.13) whereby $\mathbf{p}$ are the bath parameters (hopping and on-site energies), becomes equivalent to nonequilibrium cluster DMFT. Generalization of the SFA condition to nonequilibrium should be, in principle, obtained by replacing g_{0cc} with Σ_h in (3.13).

A second systematic improvement of this nonequilibrium VCA approach consists in increasing the cluster size L_c. This can be done in two ways: (i) by extending the boundaries of the central region in y direction and thus treating more correlated sites exactly [98] and (ii) by extending the boundaries in x direction to include an increasing number of uncorrelated lattice sites, i.e., taking $L_{cx} > \bar{L}_{cx}$, *cf.* Fig. 3.1. This amounts to taking into account to some degree the V-induced renormalization of the self-energy.

3.3 Model

Next, we present an application of the nonequilibrium VCA method described in Sec. 3.2. Specifically, we study nonlinear transport properties across an extended correlated region (denoted as c in Fig.3.1), which we take to be a Hubbard chain ($\bar{L}_{cx} = 1$) or a Hubbard ladder ($\bar{L}_{cx} = 2$) with nearest-neighbor hoppings t_x and t_y, on-site interaction U, on-site energy ϵ_c, and chemical potential μ_c

$$\bar{h}_c = \sum_{\langle i,j\rangle,\sigma} t_{ij} c^\dagger_{i\sigma} c_{j\sigma} + U \sum_i \hat{n}_{i\uparrow}\hat{n}_{i\downarrow} + (\epsilon_c - \mu_c) \sum_{i,\sigma} \hat{n}_{i\sigma} \ ,$$

in usual notation, and where $t_{ij} = t_x$ ($t_{ij} = t_y$) for i and j being nearest neighbors in x direction (y direction). The leads (shaded regions in Fig. 3.1) are described by two-dimensional semi-infinite tight-binding models with nearest-neighbor hopping

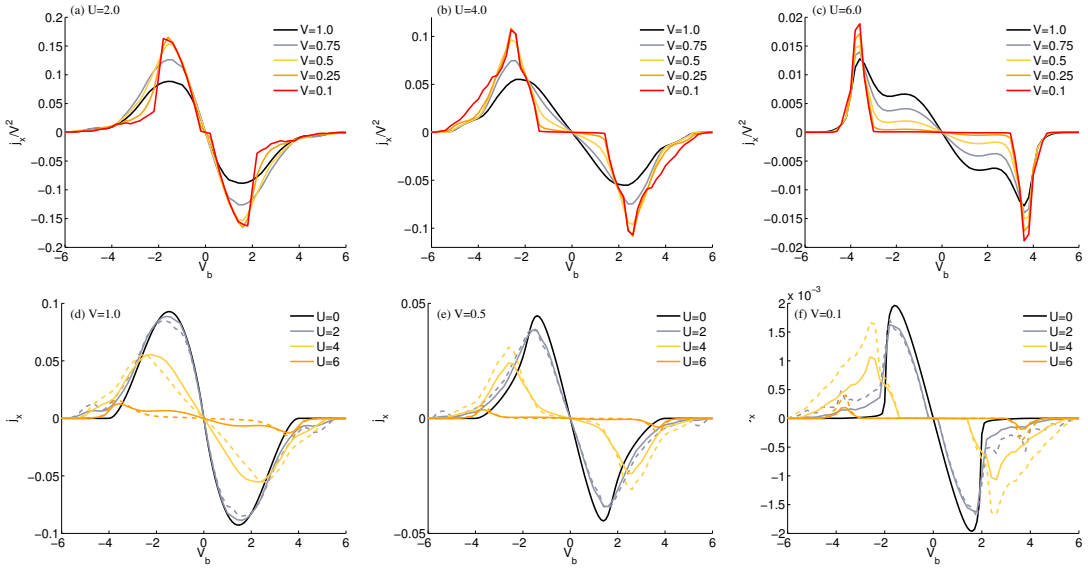

Figure 3.2: (Color online) Steady-state current density j_x versus bias voltage V_b for a correlated two-leg ladder ($\bar{L}_{cx} = 2$). First row shows j_x normalized by V^2 as function of V_b evaluated for different values of V and of the interaction (a) $U = 2.0$, (b) $U = 4.0$, and (c) $U = 6.0$. Second row shows the U dependence of the current for different values of the hopping $V = V_{lc} = V_{rc}$ from the leads to the correlated region (d) $V = 1.0$, (e) $V = 0.5$, and (f) $V = 0.1$. Solid (dashed) lines represent results for the current between the left lead and the central region (between two in x direction adjacent sites inside the central region), i.e., evaluated with G^K_{lc} (G^K_{cc}), see text for details. Results are obtained by using a reference Hamiltonian h consisting of disconnected clusters of size $L_c = L_{cx} \times L_{cy} = 2 \times 6$.

t_L, on-site energies ϵ_l and ϵ_r, and chemical potentials μ_l and μ_r for the left and right lead, respectively. We apply a bias voltage V_b to the leads by setting $\mu_r = \epsilon_r = V_b/2$ and restrict to the particle-hole symmetric case where $\epsilon_c = -U/2$, $\mu_c = 0$, $\epsilon_r = -\epsilon_l$, and $\mu_l = -\mu_r$. For simplicity, we neglect the long-range part of the Coulomb interaction. Under some conditions, this can be absorbed within the single-particle parameters of the Hamiltonian, in a mean-field sense. [57]

As discussed above, the unperturbed Hamiltonian h does not necessarily coincide with the physical partition into leads and correlated region. h is obtained by tiling the total system into small clusters as illustrated in Fig. 3.1, as well as by adding an intracluster variational term Δh.

In the present work Δh describes a correction Δt_x to the intra-ladder hopping. Further options could include, for instance, a site-dependent change in the on-site energy $\Delta\epsilon_c(x)$. Particle-hole symmetry can be preserved by constraining this change to be antisymmetric: $\Delta\epsilon_c(x) = -\Delta\epsilon_c(-x)$. In this paper, whose goal is to carry out a first test of the method, we restrict, for simplicity, to a single variational parameter. The choice of Δt_x as a variational parameter is motivated by the fact that this term is important for the current flowing in x direction. According to the prescription discussed above, we require the expectation value of the one-particle density matrix for nearest-neighbor indices in x direction to be the same for the unperturbed h and for the full H, i.e. evaluated with g_{cc} and with G_{cc}.

One comment about the chemical potential. In principle, when including some of the sites of the leads in h, i.e., when $L_{cx} > \bar{L}_{cx}$, then these additional sites have a chemical potential μ_c which differs from the one they would have if $L_{cx} = \bar{L}_{cx}$ (i.e., μ_l or μ_r). However, the chemical potential, of these sites does not affect the steady state, as their volume-to-surface ratio is finite. Of course, their on-site energies (ϵ_r and ϵ_l) are important.

Due to translation invariance by a cluster length L_{cy} in the y direction, it is

convenient, as in usual VCA, to carry out a Fourier transformation in y direction, with associated momenta q_y. The Green's functions g_{cc} and G_{cc}, as well as T become now functions of two momenta $q_y + Q_y$ and $q_y + Q'_y$, where Q_y and Q'_y are reciprocal superlattice vectors of which there are only L_{cy} inequivalent ones. In order to evaluate the nonequilibrium steady state, one only needs the equilibrium Green's function $g(x_{b\alpha}|q_y|z)$ of the isolated leads at the contact edge to the central region, with x coordinate equal to $x_{b\alpha}$ ($\alpha \in \{l, r\}$), and Fourier transformed in the y directions, where q_y is the corresponding momentum and z the complex frequency. For a semiinfinite nearest-neighbor tight-binding plane with hopping t_L, and on-site energy ϵ_α, this can be expressed as

$$g(x_{b\alpha}|q_y|z) = g_{c,loc}(z - 2t_L \cos q_y - \epsilon_\alpha) \ , \tag{3.14}$$

where $g_{c,loc}(z)$ is the local Green's function of a tight binding chain with open boundary conditions and with zero on-site energy. The latter can be determined analytically along the lines discussed in Ref. [109].

The model studied here, is motivated by the interest in transport across semiconductor heterostructures (see, e.g. [54, 55, 110, 111]). However, it is well known that in this case charging effects are important, also near the boundaries between the leads and the central region. Here, scattering effects produce charge density waves, which, when taking into account the long-range part of the Coulomb interaction, even in mean-field, produce a modification of the single-particle potential. In order to treat realistic structures, these effects should be included at the Hartree-Fock level at least. All these generalizations can be straightforwardly treated with the presented variational cluster method, however, in this work we focus on a first proof of concept study and application containing the essential ingredients for the investigation of the nonequilibrium steady state of strongly correlated many-body systems.

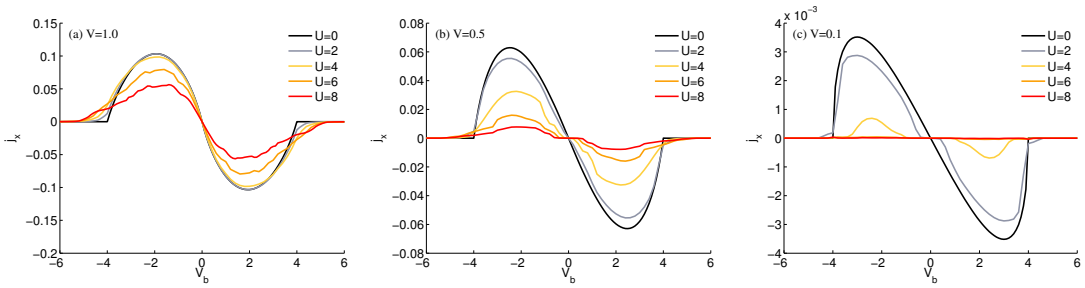

Figure 3.3: (Color online) Steady-state current density j_x as in Fig. 3.2 but for the correlated chain ($\bar{L}_{cx} = 1$). The current density is evaluated for different values of the lead to correlated region hopping (a) $V = 1.0$, (b) $V = 0.5$, and (c) $V = 0.1$, and of the interaction U, see legend. Results are obtained for reference clusters of size $L_c = L_{cx} \times L_{cy} = 3 \times 4$.

3.4 Results

We have evaluated the steady-state current density j_x of the models discussed in Sec. 3.3 as a function of the bias $V_b \equiv \epsilon_r - \epsilon_l$ between the leads at zero temperature. Simultaneously the chemical potential is adjusted to the on-site energy $\mu_\alpha = \epsilon_\alpha$, which corresponds to a rigid shift of the density of states in both leads in opposite directions.

In Fig. 3.2 we display results for the two-leg ladder ($\bar{L}_{cx} = 2$), for different values of the interaction strength $U = \{0, 2, 4, 6\}$ and lead-to-system hopping $V = \{1.0, 0.75, 0.5, 0.25, 0.1\}$. We use $\hbar = 1$ and $t_L = 1$ which sets the unity of energy. Moreover, we take the lattice constant $a = 1$. The hopping is uniform in the whole system, meaning that t_x, t_y in the correlated region and t_L of the leads are equal. The on-site energy of the correlated region is $\epsilon_c = -U/2$ corresponding to half-filling, whereas the on-site energy of the left (right) lead is equal to its chemical potential μ_l (μ_r). The unperturbed hamiltonian h describes the central

region decomposed into clusters of size $L_c = 2 \times 6$. The corresponding Green's function g_{cc} is determined exactly by Lanczos diagonalization. All results are determined self-consistently using Δt_x as variational parameter, see Sec. 3.3.

Using the Meir-Wingreen expression, Eq. (3.11), the general trend of the results for the steady-state current j_x can be discussed conveniently. At zero temperature there are only contributions to the current for $\min(\mu_l, \mu_r) < \omega < \max(\mu_l, \mu_r)$ due to the difference of the Fermi distribution functions. In particular this leads as expected to zero current for zero bias voltage V_b. With increasing bias voltage V_b the modulus of j_x initially increases. For large values of V_b it decreases again, as the overlap of the local density of states of the two leads enters the expression, which is zero if V_b is greater than the band width of the leads. Hence the local density of states of the leads along with the Fermi function act as a filter that averages the electronic excitations of the central region within a certain energy window.

In the system we are studying, the leads are modeled by semi-infinite tight binding planes. Alternatively, instead of using (3.14) one could simply put a model Green's function "by hand," as for example one which describes a Lorentzian shaped density of states. Such an unbound density of states generally leads to a finite value of the current for arbitrary bias.

The leads have a further effect on the result as they provide an inelastic broadening of the energy spectrum of the central region entering Σ^{eff}, see Eq. (3.10), which smears out details of the excitation spectrum. As far as the lead-correlated region coupling V is concerned, there are two competing effects: on the one hand, the current increases with increasing V due to the stronger coupling between the correlated region and the leads. On the other hand, details of the electronic excitations are smeared out with increasing V leading to a reduced resolution. Therefore, in order to detect the effects of strong correlations, particularly the gap, a small

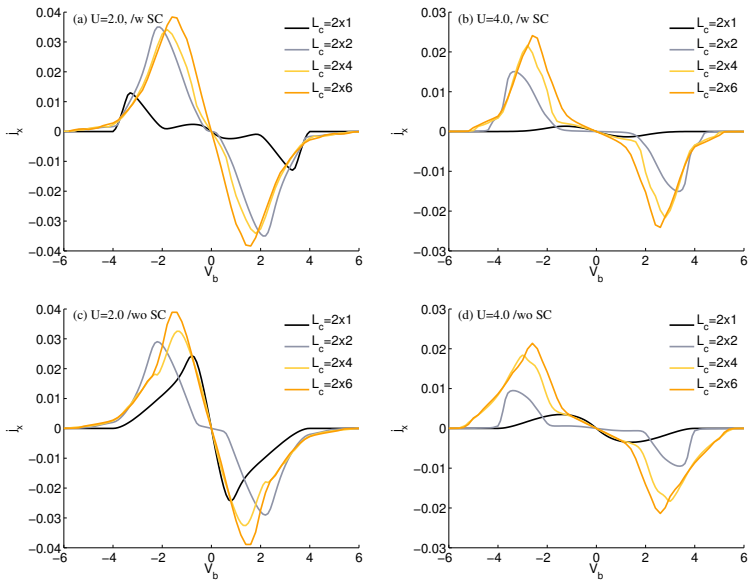

Figure 3.4: (Color online) Convergence of the steady-state current density j_x with reference cluster size $L_c = L_{cx} \times L_{cy}$ for the correlated two-leg ladder with $V = 0.5$. Results in (a), (b) are obtained by a variational adjustment of the intra-cluster hopping t_x as discussed in the text, while those of (c), (d) are obtained without modification of t_x. The values for the Hubbard interaction are $U = 2$ in [(a), (c)] and $U = 4$ in [(b), (d)].

value for V is required.

The details of the V dependence of j_x for small V can be deduced from (3.11). Here, the expression for the current has a prefactor proportional to V^4 (at least in the $L_{cx} = \bar{L}_{cx}$ case), due to the two Γ terms. On the other hand, for a gapless system, there is a V^2 term in the denominator of $|G^R_{cc}|^2$. For a gapped system, this is cut off by the energy gap E_g, so that in this case $j_x \sim V^4/E_g^2$, while $j_x \sim V^2$ for a gapless spectrum. These aspects are clearly observable in Fig. 3.2 (a)–(c), which shows the scaled current density j_x/V^2 for fixed interaction strength U but varying V. The envelope has a rotated S-like structrue due to the combined effects of the lead density of states and of the Fermi functions. The overall size of the structures deceases with increasing Hubbard interaction U and the gap becomes more pronounced with decreasing V.

Next we will analyze a bit more in detail the results for the current across the Hubbard ladder in Fig. 3.2. Increasing the interaction strength U in the correlated region leads to a suppression of the current and the opening of a gap, which is best oberserved in (c). For $U = 4$ the maximum of the current density is roughly reduced by a factor of two as compared to the noninteracting case, whereas for $U = 6$ the current is almost one order of magnitude smaller as compared to the noninteracting system, see Fig. 3.2 (d)–(f).

Finally, we want to address the the difference between the solid lines and dashed lines in the the panels (a)–(c) of Fig. 3.2, which represent the current density evaluated on a bond connecting the leads to the central region, or on a bond within the two-leg ladder. Due to the stationary condition, the two results should coincide. However, our calculations shows a slight discrepancy between them, which is due to the fact that the method is not completely conserving and, thus, the continuity equation is not completely fulfilled. However, from our results we see that the deviation from the continuity equation is quite small. We expect this

discrepancy to be reduced upon improving the optimization with the introduction of additional variational parameters.

In Fig. 3.3 we show the steady-state current density j_x across the correlated chain ($\bar{L}_{cx} = 1$) as a function of the bias voltage. The parameters are the same as in the case of the two-leg ladder, however, the central region is decomposed into clusters of size $L_c = 3 \times 4$, where also sites of the leads are taken into account to improve the results. The half-filled Hubbard chain is gapped as well. As for the two-leg ladder, the gap behavior can be better seen in the current-voltage characteristics for smaller values of V, in our case for $V = 0.1$. In contrast, for strong coupling $V = 1.0$, (a), no gap behavior can be seen in the current due to the strong hybridization with the leads.

For strong values of the coupling V between leads and correlated region ($V = 1.0$), (a), the current is significant for all values of the interaction U. However, with decreasing V, (b)–(c), the current is strongly suppressed for large interaction U. Importantly, for the correlated chain the continuity equation is always strictly fulfilled. In other words, there is no difference between j_x evaluated on a inter-cluster bond between the leads and the cluster, or on an intracluster bond. This is due to the absence of vertex corrections at the uncorrelated sites.

Next, we study the convergence of our results with the size of the cluster, as well as the effect of the self-consistency condition for the two-leg ladder and $V = 0.5$. Results are depicted in Fig. 3.4 for two different values of the Hubbard interaction, namely $U = 2$ [(a), (c)] and $U = 4$ [(b), (d)]. We do not plot results of the convergence analysis for $U = 6$, since for this large U the current is already rather small, as can be seen in Fig. 3.2 (d)–(f). Results in (a) and (b), first row, are obtained by adjusting Δt_x self-consistently, as described in Sec. 3.3, whereas (c) and (d), second row, shows results without self-consistency, i.e., with $\Delta t_x = 0$. Results show that the self-consistency procedure improves the results, as the convergence

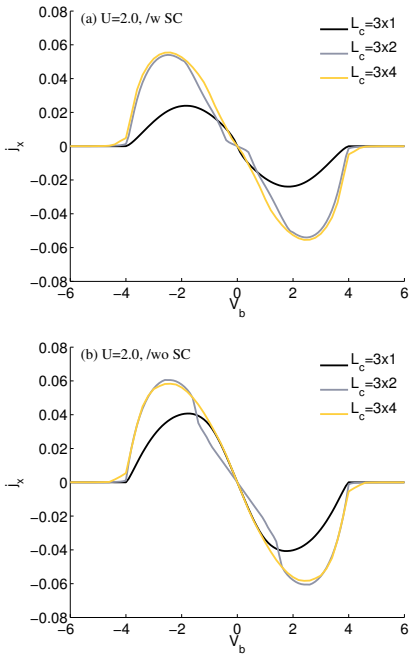

Figure 3.5: (Color online) Convergence of the steady-state current density j_x with reference cluster size $L_c = L_{cx} \times L_{cy}$ for the correlated chain. Results in (a) fulfill the self-consistency condition (3.13), whereas results in (b) do not. The parameters are $U = 2$ and $V = 0.5$.

for j_x is faster with increasing cluster size as compared to the case without self-consistency. Generally, we observe pronounced finite size effects for very small clusters up to 2×4, and convergence seems to be reached for the 2×6 cluster.

We now repeat the same analysis for the correlated chain. The corresponding current densities for the parameters $U = 2$ and $V = 0.5$ are shown in Fig. 3.5 for different cluster sizes. Results shown in (a) are with self-consistency procedure (3.13), whereas the results shown in (b) are without. In the present case, where we consider transport across a strongly correlated chain, convergence is achieved very quickly with increasing cluster size. Therefore, there is no sensible difference be-

tween results obtained with or without self-consistency, apart for the pathological case $L_c = 3 \times 1$ (see below).

Results obtained for the two-leg ladder and for the chain show that cluster geometries with $L_{cy} = 1$ provide results far from convergence, even with self-consistency. For the chain this is probably due to the degeneracy of the cluster ground state. For the ladder, it seems that using as starting point the 2×1 dimer exaggerates the gap. But besides these data obtained from admittedly very small clusters, results converge quickly as a function of cluster sizes, especially when the hopping in x direction is used as a variational parameter.

3.5 Conclusions

In this paper we have presented a novel approach to treat strongly correlated systems in the nonequilibrium steady state. The idea is based on the variational cluster approach extended to the Keldysh formalism. For the present approach the expression for the current resembles the corresponding Meir-Wingreen formulas. As in the original Meir-Wingreen approach, which is also the basis for nonequilibrium density-functional based calculations, we directly address the steady state behavior of a device coupled to infinite leads. The latter is necessary for the system to reach a well-defined steady state.

The present nonequilibrium extension is in a similar spirit to the equilibrium self-energy functional approach, in which one "adds" single-particle terms to the cluster Hamiltonian which is then solved exactly, and "subtract" them perturbatively. [90, 91] The values of the parameters are determined by an appropiate requirement which in the end amounts to optimizing the unperturbed state with respect to the perturbed one.

There is a certain freedom in choosing the most appropriate self-consistency

criterion. Here we have required the operators associated with the variational parameters to have the same expectation values in the unperturbed and in perturbed state. Certainly, an interesting alternative would be to generalize the variational criterion provided by the self-energy functional approach [95] to the nonequilibrium case. This will be obtained by a suitable generalization of the Euler equation (Eq. (7) of Ref. [95]) to the Keldysh contour, i.e., by replacing g_{0cc} with the self-energy Σ_h in (3.13) Work along these lines is in progress.

The advantage of the present variational condition (3.13) is that it is computationally less demanding, as one just needs to evaluate cluster single-particle Green's functions. Which one of the two conditions gives more accurate results cannot be stated a priori and should be explicitly checked.

In any case, both methods, the self-energy functional approach and the present one, become equivalent to (cluster) dynamical mean-field theory in the case in which an infinite number of variational parameters is suitably taken (see Appendix 3.6.1).

In general, we expect results to improve when more variational parameters are taken into account. In particular, when evaluating the current across the central region, it would be useful if a current was already flowing in the cluster. This can be achieved by adding a complex variational hopping between the end points of the cluster, and of course remove it perturbatively. The corresponding variational condition would contain the interesting requirement that the current flow in this modified cluster be the same as in steady state.

The model studied here, is motivated by the interest in transport across semiconductor heterostructures (see, e.g. [54, 55, 110, 111]). However, it is well known that in this case charging effects are important, also near the boundaries between the leads and the correlated region. Here, scattering effects produce charge density waves, which, when taking into account the long-range part of the Coulomb

interaction, even in mean-field, produce a modification of the single-particle potential. In order to treat realistic structures, these effects should be included at the Hartree-Fock level at least. All these generalizations can be straightforwardly treated with the presented variational cluster method, however, in this work we focus on a first proof of concept study and application containing the essential ingredients for the investigation of the nonequilibrium steady state of strongly correlated many-body systems.

3.6 Appendix

3.6.1 Connection to (cluster) Dynamical Mean-Field Theory

Here, we show that the self-consistent condition (3.13) provides a bridge to (cluster) DMFT, when an increasing number of noninteracting bath sites is included in the cluster Hamiltonian. Notice that these are "auxiliary" baths and are not related to the leads. Concretely, the "auxiliary" Hamiltonian δh contains a set of hoppings with amplitudes v_n connecting the central region with a corresponding set of uncorrelated bath sites. Therefore, the couplings v_n to the bath sites are included in the reference (unperturbed) Hamiltonian h, but are "subtracted perturbatively," so that they are absent from the target Hamiltonian H.

Now, since g_{0cc} is cluster-local, a solution to (3.13) is obviously given by (3.12). However, this solution can generally not be obtained with a finite number of parameters. As in usual equilibrium (cluster) DMFT, [93] (3.12) can thus be solved via an iterative procedure defined by

$$\begin{aligned} g_{0cc,new}^{-1} &= \left(\mathcal{P}(G_{cc})\right)^{-1} + \Sigma_h \\ \Sigma_h &= g_{0cc,old}^{-1} - g_{cc}^{-1} \,. \end{aligned} \tag{3.15}$$

It is, thus, sufficient to show that an arbitrary $g_{0cc,new}$ can be obtained by coupling

the cluster to a noninteracting bath with suitably chosen bath parameters. For the retarded and advanced Green's functions, the procedure is the same as in equilibrium. The Keldysh part is slightly more complicated. In order to show that an aribrary $g_{0cc,new}$ can be realized, one introduces the hybridization function

$$\Delta(\omega) = \begin{pmatrix} \Delta^R(\omega) & \Delta^K(\omega) \\ 0 & \Delta^A(\omega) \end{pmatrix} , \tag{3.16}$$

where the Δ^R, Δ^A, and Δ^K are matrices in the cluster sites. Similarly to equilibrium DMFT $g_{0cc,new}$ is expressed as

$$g^{-1}_{0cc,new} = g^{-1}_{0cc,0} - \Delta(\omega) . \tag{3.17}$$

Here, $g^{-1}_{0cc,0}$ is the "bare" noninteracting cluster Green's function, i.e., the one with neither baths nor variational parameters.

One then introduces a bath of noninteracting and initially decoupled sites with energies ϵ_n and occupation probabilities p_n. A generic nonequilibrium $\Delta(\omega)$ is produced by switching on the corresponding hybridizations v_n (each one is a vector in cluster sites) at a certain time in the past, and waiting for the onset of the steady state. The bath parameters have a one-to-one correspondence with the bath spectral function (matrix)

$$A_{bath}(\omega) = \sum_n v_n v_n^\dagger \delta(\omega - \epsilon_n) \tag{3.18}$$

and with its distribution function $s_{bath}(\omega)$ defined as

$$A_{bath}(\omega)\ s_{bath}(\omega) = \sum_n v_n v_n^\dagger \delta(\omega - \epsilon_n)(1 - 2\ p_n) . \tag{3.19}$$

In order to produce a given $\Delta(\omega)$ these two functions must be fixed by the conditions

$$-\ 2i\pi\ A_{bath}(\omega) = \big(\Delta^R(\omega) - \Delta^A(\omega)\big) \tag{3.20}$$

and

$$-2i\pi\ A_{bath}(\omega)\ s_{bath}(\omega) = \Delta^K(\omega)\ . \tag{3.21}$$

which can be easily seen to lead to (3.16)

4 Extended self-energy functional approach for strongly-correlated lattice bosons in the superfluid phase

Enrico Arrigoni Institute of Theoretical and Computational Physics, Graz University of Technology, 8010 Graz, Austria

Michael Knap Institute of Theoretical and Computational Physics, Graz University of Technology, 8010 Graz, Austria

Wolfgang von der Linden Institute of Theoretical and Computational Physics, Graz University of Technology, 8010 Graz, Austria

Among the various numerical techniques to study the physics of strongly correlated quantum many-body systems, the self-energy functional approach (SFA) has become increasingly important. In its previous form, however, SFA is not applicable to Bose-Einstein condensation or superfluidity. In this paper we show how to overcome this shortcoming. To this end we identify an appropriate quantity, which we term D, that represents the correlation correction of the condensate order parameter, as it does the self-energy for the Green's function. An appropriate

functional is derived, which is stationary at the exact physical realizations of D and of the self-energy. Its derivation is based on a functional-integral representation of the grand potential followed by an appropriate sequence of Legendre transformations. The approach is not perturbative and therefore applicable to a wide range of models with local interactions. We show that the variational cluster approach based on the extended self-energy functional is equivalent to the "pseudoparticle" approach introduced in Chap. 2. We present results for the superfluid density in the two-dimensional Bose-Hubbard model, which show a remarkable agreement with those of Quantum-Monte-Carlo calculations.

4.1 Introduction

Seminal experiments with ultracold gases of atoms trapped in optical lattices shed new light on strongly-correlated many body systems. [42–44] In these experiments specific lattice Hamiltonians can be engineered and investigated with a remarkable high level of control, making quantum mechanical interference effects observable on a macroscopic scale. Most important as well as fundamental is the quantum phase transition of strongly correlated lattice bosons from the localized Mott phase to the delocalized superfluid phase. In the superfluid phase a macroscopic fraction of the particles condenses into one quantum mechanical state, thus, forming a Bose-Einstein condensate, where the number of particles in the condensate is not necessarily equal to the number of superfluid particles. In experiments with ultracold gases of atoms trapped in optical lattices, the condensate density can be extracted from time-of-flight images, [43] which are related to the momentum distribution of the confined particles. Importantly, the finite expansion time of the particle cloud has to be taken into account when drawing the connection between these time-of-flight images and the true momentum distribution. [112–115]

However, it is probably even more challenging to measure the superfluid density itself, as it is not a ground state property but rather related to the response of the system to a phase twisting field. [116] Interestingly, only very recently for Bose gases without the periodic lattice potential an optical method has been proposed to extract the superfluid density. This experiment creates a vector potential, that imposes angular momentum on normal fluid particles, while superfluid particles stay at rest. [117]

In a previous work, we extended the variational cluster approach (VCA), which is capable to deal with strongly-correlated many body systems without broken symmetry to the superfluid phase of lattice bosons. [91] Originally, VCA has been formulated for the normal Mott phase of lattice bosons in Ref. [118] within the so-called self-energy functional approach (SFA), which was previously introduced for interacting fermionic systems. [119, 120] Our extension to the superfluid phase in Ref. [91] follows a different path, and is based on the so-called "pseudoparticle" formalism. Within this approach we obtained the expressions for the superfluid order parameter, the anomalous Green's function, and the grand potential, which is the starting point for the variational principle, see Eq. (1), (33), and (2) in this reference.

It should be pointed out that, while the pseudoparticle formalism is equivalent to VCA in the normal phase of both bosonic [91] and fermionic [121] systems, it lacks the rigorous theroretical framework provided by SFA. In particular, there is no genuine variational principle explaining why one should look for a saddle point in the grand potential. The goal of the present paper is to put the results obtained within the pseudoparticle approach into a rigorous framework by developing an extended self-energy functional approach, which is capable to deal with the bosonic superfluid phase.

From the present work it will become clear, that this extension is not straightfor-

ward, as it involves a precise sequence of Legendre transformations with suitably chosen variables. In the search for the appropriate set of transformations the knowledge of the final results provided by pseudoparticle formalism proves to be useful. This fact emphasizes the advantage of the heuristic, yet straightforward, pseudoparticle approach to formulate extensions of VCA. [91]

The extended SFA formulated in the present paper yields the same expressions for the superfluid order parameter, for the Nambu Green's function, and for the grand potential, as obtained from the pseudoparticle approach. While this might not seem to be surprising, since we were guided by the very results of the pseudoparticle approach, we argue below, that our SFA extension presented here is unambiguous. The most important step in this SFA extension is to find a quantity, which we call D, which is the companion of the self-energy in the superfluid phase. Correspondingly, one has to find an appropriate universal functional of this quantity and of the self-energy, which generates the superfluid order parameter and the Green's function.

As an application, we present an evaluation of the superfluid density within this extended VCA, by the usual method of introducing a phase twisting field, which is equivalent to the helicity modulus [122] and to winding numbers in quantum Monte Carlo (QMC) algorithms. [123, 124] We evaluate the superfluid density for the two-dimensional Bose-Hubbard (BH) model [125] and find a remarkably excellent agreement with QMC results.

This article is organized as follows. In Sec. 4.2 we extend SFA to the superfluid phase and obtain the corresponding extended self-energy functional, along with the appropriate variable describing superfluidity. The evaluation of the superfluid density within this extended VCA is presented in Sec. 4.3 and applied to the BH model in two dimensions. The VCA results are compared with unbiased QMC results showing excellent agreement. Finally, we conclude and summarize our

findings in Sec. 4.4.

4.2 Self-energy functional approach

Let us recall the key idea of SFA due to M. Potthoff. [119] The starting point is an appropriate functional

$$\hat{\Omega}[\Sigma, G_0^{-1}, H_U] \equiv \hat{\mathcal{F}}[\Sigma, H_U] + \hat{\mathcal{E}}[\Sigma, G_0^{-1}] \,, \tag{4.1}$$

which consists of a functional $\hat{\mathcal{F}}$ of the self-energy, the Legendre transform of the Luttinger-Ward functional, which is universal in the sense that it depends on the interaction part (H_U) of the Hamiltonian but not on the single particle part. The latter enters via the free Green's function G_0^{-1} in the second functional, which is explicitly known

$$\hat{\mathcal{E}}[\Sigma, G_0^{-1}] \equiv -\beta \,\mathrm{tr}\ln(\Sigma - G_0^{-1})$$

The functional $\hat{\Omega}[\Sigma, G_0^{-1}, H_U]$ has three key features, which are crucial for VCA.

a) The non-universal part $\hat{\mathcal{E}}$ enters additively in form of a known functional and the many-body aspects are described by a universal functional independent of the single particle Hamiltonian, or, equivalently, independent of G_0^{-1}.

b) The self-energy of the physical system, characterized by H_U and G_0^{-1} is a stationary point of the functional $\hat{\Omega}$ with respect to Σ.

c) The value of $\hat{\Omega}$ at the stationary point is equal to the thermodynamic grand potential.

Given these properties, one can construct a parametric family of Hamilton operators based on the same interaction part (reference systems), for which the ther-

modynamic grand potential, the Green's function and the self-energy can be determined exactly. This allows to determine the exact self-energy functional for self-energies accessible by the reference systems. In this very subspace, the self-energy functional in Eq. (4.1) for the physical system is replaced by that of the reference system. The stationarity condition in turn allows to determine the Green's function and self-energy of the physical system.

Our goal is to generalize this approach to the superfluid phase as well. Besides the self-energy, which is the interaction correction of the inverse Green's function, we need the corresponding companion that describes the interaction correction to the order parameter, which we call D.

Once the appropriate form of D has been determined, we need a functional

$$\hat{\Omega}_s[\Sigma, D, F, G_0^{-1}, H_U] \equiv \hat{\mathcal{F}}[\Sigma, D, H_U] + \hat{\mathcal{E}}[\Sigma, D, G_0^{-1}, F] \;,$$

in the self-energy Σ and D with the following features.

a) $\hat{\mathcal{F}}$ is again a universal functional, now in Σ and D. The non-universal part $\hat{\mathcal{E}}$ is explicitly known and carries the dependence on G_0^{-1} and the symmetry breaking source-field F.

b) The functional is again stationary at the exact self-energy Σ and the exact D of the physical system, characterized by H_U, G_0^{-1} and F.

c) The value of $\hat{\Omega}_s$ at the stationary point is equal to the thermodynamic grand potential.

The sought-for functional $\hat{\Omega}_s$, to be derived in this section, will turn out to be (see below for a definition of the quantities)

$$2\beta\hat{\Omega}_s[\Sigma,\, D, G_0^{-1}, F] = \hat{\mathcal{F}}[\Sigma, D] + \hat{\mathcal{E}}[\Sigma,\, D, G_0^{-1}, F] \tag{4.2}$$

$$\begin{aligned}\hat{\mathcal{E}}[\Sigma,\, D, G_0^{-1}, F] \equiv{}& \beta\,\mathrm{Tr}\ln[(G_0^{-1} - \Sigma)\; G_\infty] \\ &+ (\bar{D} - \bar{F})(G_0^{-1} - \Sigma)^{-1}(D - F) \;.\end{aligned} \tag{4.3}$$

In the normal phase, it is identical to the functional introduced by Potthoff. The additional factor 2 is due to the Nambu Green's functions. Moreover, the expression for the grand potential obtained with the help of a so-called reference system, see Eq. 4.30 below, is identical to the one obtained within the pseudoparticle approach. [91]

4.2.1 Derivation of the grand potential functional

We start out from the partition function Z of a bosonic many-body system, which in a functional integral representation reads

$$Z = \int \mathcal{D}A \; e^{-S} \; , \tag{4.4}$$

where S is the action, which in general can be written as [126]

$$\begin{aligned} S = &- \frac{1}{2} \int d\tau \int d\tau' \, \bar{A}(\tau') \, G_0^{-1}(\tau', \tau) \, A(\tau) \\ &- \int d\tau \left[\bar{F}(\tau) \, A(\tau) - H_U(A(\tau)) \right] \; . \end{aligned} \tag{4.5}$$

In view of treating the superfluid phase we have adopted a Nambu notation in which the bosonic fields are expressed in a vector representation

$$A(\tau) \equiv \begin{pmatrix} a_1(\tau) \\ \vdots \\ a_N(\tau) \\ \bar{a}_1(\tau) \\ \vdots \\ \bar{a}_N(\tau) \end{pmatrix} \; . \tag{4.6}$$

The indices 1 through N denote the corresponding single-particle orbitals (for example, lattice sites) where the boson operators act, and $a_i(\tau)$ ($\bar{a}_i(\tau)$) are the

fields associated with the annihilation (creation) of a boson in the orbital i. The adjoint field is defined as

$$\bar{A}(\tau) \equiv (\bar{a}_1(\tau), \cdots, \bar{a}_N(\tau), a_1(\tau), \cdots, a_N(\tau)) \ . \tag{4.7}$$

It can be expressed in terms of $A(\tau)$ with the help of the matrix $\mathcal{T}$, which exchanges the first N entries of a vector with the last N ones:

$$\bar{A}(\tau) = A(\tau)^T \mathcal{T} \ . \tag{4.8}$$

The operator $\mathcal{T}$ has the properties $\mathcal{T}^2 = \mathbb{1}$, and $\mathcal{T} = \mathcal{T}^T$. The action in Eq. (4.5) also contains the source fields

$$\bar{F} \equiv \left(f_1, \cdots f_N, \bar{f}_1, \cdots, \bar{f}_N\right) \quad \text{and} \quad F = \mathcal{T}\bar{F}^T \ ,$$

which are zero for the physical system of interest, the boson interaction described by H_U, as well as the $2N \times 2N$ noninteracting Green's function matrix $G_0(\tau', \tau)$. Eq. (4.4) with Eq. (4.5) defines the corresponding grand potential as a functional of G_0^{-1} and F

$$\hat{\tilde{\Omega}}_s[G_0^{-1}, F] \equiv -\frac{1}{\beta} \ln \hat{Z} \, , \tag{4.9}$$

where β is the inverse temperature. Here and in the following, we mark functionals with a hat " $\hat{}$ ", and omit their arguments whenever they are obvious. The noninteracting Green's function has the matrix structure (see App. 4.5.1)

$$G_0^{-1}(\tau', \tau) = -\delta(\tau - \tau') \begin{pmatrix} \partial_\tau + \mathbf{t} & 0 \\ 0 & -\partial_\tau + \mathbf{t} \end{pmatrix} \ , \tag{4.10}$$

where $\mathbf{t}$ is the single-particle Hamiltonian matrix.

In the following, we carry out a sequence of Legendre transformations starting from $\hat{\tilde{\Omega}}_s$, ultimately leading to a universal functional $\hat{\mathcal{F}}[\Sigma, D]$ of the self-energy Σ and of a suitable quantity D defined in Eq. (4.21a). The functional $\hat{\mathcal{F}}$ is the generalization of the self-energy functional [118–120] to the superfluid phase, where a

nonvanishing expectation value $\mathcal{A}(\tau)\equiv\langle A(\tau)\rangle$ of the boson operators A exists. The functional $\hat{\mathcal{F}}$ has the properties, see Eq. (4.23), that its functional derivatives with respect to Σ and D yield the disconnected Green's function, and the expectation value $\mathcal{A}$, respectively. This procedure is inspired by Ref. [127] and extends that approach to the treatment of the superfluid phase.

We first determine the conjugate variables to G_0^{-1} and to the source fields F. The functional derivative of $\hat{\tilde{\Omega}}_s$ with respect to the noninteracting Green's function yields [126] (see App. 4.5.1)

$$\begin{aligned}
2\beta\frac{\delta\hat{\tilde{\Omega}}_s}{\delta G_{0\,ji}^{-1}(\tau',\tau)} &= -\frac{2}{\hat{Z}}\frac{\delta}{\delta G_{0\,ji}^{-1}(\tau',\tau)}\int\mathcal{D}A\times \\
&\quad\times\exp\Big\{\frac{1}{2}\int d\tilde{\tau}\int d\tilde{\tau}'\,\bar{A}_l(\tilde{\tau})\,G_{0\,ll'}^{-1}(\tilde{\tau},\tilde{\tau}')\,A_{l'}(\tilde{\tau}') \\
&\quad+\int d\tilde{\tau}[\bar{F}_l(\tilde{\tau})\,A_l\,(\tilde{\tau})-H_U(\bar{a},\,a)]\Big\} \\
&= -\frac{1}{\hat{Z}}\int\mathcal{D}A\,\bar{A}_j(\tau')\,A_i\,(\tau)\exp\left[-S\right] \\
&\equiv \hat{\mathrm{G}}_{\mathrm{disc},ij}(\tau,\tau')\;.
\end{aligned}$$

Here $\hat{\mathrm{G}}_{\mathrm{disc},ij}(\tau,\tau')$ is the disconnected interacting time-ordered Green's function. Along with the definition of the connected Green's function $\hat{G}[G_0^{-1},F]$ we obtain

$$2\beta\frac{\delta\hat{\tilde{\Omega}}_s[G_0^{-1},F]}{\delta G_0^{-1}} = \hat{\mathrm{G}}_{\mathrm{disc}} \equiv \hat{G}-\hat{\mathcal{A}}\hat{\bar{\mathcal{A}}}\;. \tag{4.11a}$$

For the functional derivative with respect to F we obtain similarly

$$2\beta\frac{\delta\hat{\tilde{\Omega}}_s[G_0^{-1},F]}{\delta\bar{F}} = -2\hat{\mathcal{A}}[G_0^{-1},F]\;. \tag{4.11b}$$

The two functionals $\hat{G}[G_0^{-1},F]$ and $\hat{A}[G_0^{-1},F]$ defined in Eq. (4.11) provide the exact Green's function G and order parameter A for a given noninteracting Green's function G_0^{-1} and source field F of the system. The first step toward the universal

functional consists in a Legendre transformation replacing the variables F with $\mathcal{A}$. To this end, we invert [128] the relation Eq. (4.11) making F a functional $\hat{F}[G_0^{-1}, \mathcal{A}]$ and introduce

$$\hat{\Xi}[G_0^{-1},\, \mathcal{A}] = 2\beta\hat{\tilde{\Omega}}_s + 2\hat{\tilde{F}}\mathcal{A}\ , \tag{4.12}$$

where, as usually in Legendre transformations, the functional dependence on F has been eliminated in favor of $\mathcal{A}$ by using the inverse function. It is straightforward to show that the corresponding functional derivatives give

$$\frac{\delta\hat{\Xi}}{\delta 2\mathcal{A}} = \hat{\tilde{F}}[G_0^{-1}, A]\ , \quad \frac{\delta\hat{\Xi}}{\delta G_0^{-1}} = \hat{\mathrm{G}}_{\mathrm{disc}}[G_0^{-1}, A]\ .$$

Next, we modify the functional in the following way

$$\hat{\tilde{\Xi}}[G_0^{-1},\, \mathcal{A}] = \hat{\Xi} + \bar{\mathcal{A}}G_0^{-1}\mathcal{A}\ , \tag{4.13}$$

such that we obtain the connected Green's function from the functional derivative with respect to G_0^{-1}. In total we have

$$\frac{\delta\hat{\tilde{\Xi}}}{\delta 2\mathcal{A}} = \hat{\tilde{F}}[G_0^{-1}, A] + \bar{\mathcal{A}}G_0^{-1}\ , \tag{4.14}$$

$$\frac{\delta\hat{\tilde{\Xi}}}{\delta G_0^{-1}} = \hat{\mathrm{G}}_{\mathrm{disc}} + \mathcal{A}\bar{\mathcal{A}} = \hat{G}[G_0^{-1}, A]\ . \tag{4.15}$$

The second step is a Legendre transformation replacing the variable G_0^{-1} with G

$$\hat{\Pi}[G,\, \mathcal{A}] = \hat{\tilde{\Xi}} - \beta\,\mathrm{Tr}(G\,\hat{G}_0^{-1} - \mathbb{1})\ , \tag{4.16}$$

where we have expressed $\hat{G}_0^{-1}$ as a functional of G and $\mathcal{A}$, by inverting Eq. (4.15). [126,128] We subtract an "infinite" constant $\beta\,\mathrm{Tr}\,\mathbb{1}$ in order to keep $\hat{\Pi}[G,\, \mathcal{A}]$ finite. The functional derivatives of the new functional are

$$\frac{\delta\hat{\Pi}}{\delta 2\mathcal{A}} = \hat{\tilde{F}} + \bar{\mathcal{A}}\hat{G}_0^{-1}\ , \quad \frac{\delta\hat{\Pi}}{\delta G} = -\hat{G}_0^{-1}\ .$$

Now, we modify the functional such that we get the self-energy from the functional derivative (see App. 4.5.1)

$$\hat{\tilde{\Pi}}[G,\, \mathcal{A}] = \hat{\Pi} + \beta\,\mathrm{Tr}\ln\left(G/G_\infty\right)\ . \tag{4.17}$$

This gives

$$\frac{\delta\hat{\tilde{\Pi}}}{\delta 2\mathcal{A}} = \hat{\bar{F}} + \bar{\mathcal{A}}\hat{G}_0^{-1} , \quad \frac{\delta\hat{\tilde{\Pi}}}{\delta G} = \hat{\Sigma} \tag{4.18a}$$

$$\hat{\Sigma} \equiv G^{-1} - \hat{G}_0^{-1} . \tag{4.18b}$$

Here we have used the Dyson equation as defining equation for the self-energy. Furthermore, we carry out a third Legendre transformation replacing G with Σ in the usual way. Thus we introduce

$$\hat{P}[\Sigma,\, \mathcal{A}] = \hat{\tilde{\Pi}} + \beta \,\mathrm{Tr}\, \Sigma\, \hat{G} \tag{4.19}$$

with the properties

$$\frac{\delta\hat{P}}{\delta 2\mathcal{A}} = \hat{\bar{F}} + \bar{\mathcal{A}}\hat{G}_0^{-1} , \quad \frac{\delta\hat{P}}{\delta\Sigma} = \hat{G} .$$

We modify this functional once more so that its derivative yields a new function D, which will be the companion of the self-energy in our extended self-energy approach

$$\hat{\tilde{P}}[\Sigma,\, \mathcal{A}] = \hat{P} - \bar{\mathcal{A}}\Sigma\mathcal{A} . \tag{4.20}$$

The functional derivatives yield

$$\frac{\delta\hat{\tilde{P}}}{\delta 2\mathcal{A}} = \hat{\bar{F}} + \bar{\mathcal{A}}\hat{G}_0^{-1} - \bar{\mathcal{A}}\Sigma = \hat{\bar{F}} + \bar{\mathcal{A}}\hat{G}^{-1} \equiv \hat{\bar{D}} , \tag{4.21a}$$

$$\frac{\delta\hat{\tilde{P}}}{\delta\Sigma} = \hat{G} - \mathcal{A}\bar{\mathcal{A}} = \hat{G}_{\mathrm{disc}} . \tag{4.21b}$$

Before proceeding, let us discuss the meaning of the function D introduced in Eq. (4.21a). When extending SFA to the superfluid phase one is looking for a quantity, which is related to the condensed order parameter and which plays a similar role as the self-energy, in that it describes the deviation between the interacting and non-interacting case. Thus, this quantity should vanish in the noninteracting case ($H_U = 0$). The reason is that SFA will eventually amount to an approximation for Σ and D, and we require this approximation to become

exact for $H_U = 0$. Finally, D must obviously vanish in the normal phase. The expression in Eq. (4.21a) has precisely these features, since $\bar{\mathcal{A}}_0 = -\bar{F}G_0$, which is straightforwardly determined from the Gaussian integral for $H_U = 0$ in Eq. (4.5). Interestingly, the pseudoparticle approach, presented in Ref. [91], and which is based on an intuitive, yet heuristic approximation, provides the same form of D as given in Eq. (4.21a).

The final Legendre transformation replacing $\mathcal{A}$ with D yields the desired functional of the self-energy and D. It represents the generalization of the self-energy functional ($F[\Sigma]$ of Refs. [119] and [118]) to the superfluid phase

$$\hat{\mathcal{F}}[\Sigma,\, D] = \hat{\tilde{P}} - 2\bar{D}\hat{\mathcal{A}} \tag{4.22}$$

and has the properties

$$\frac{\delta\hat{\mathcal{F}}}{\delta\bar{D}} = -2\hat{\mathcal{A}}[\Sigma, D]\ , \quad \frac{\delta\hat{\mathcal{F}}}{\delta\Sigma} = \hat{\mathrm{G}}_{\mathrm{disc}}[\Sigma, D]\ . \tag{4.23}$$

Similarly to $F[\Sigma]$ from Refs. [119] and [118], $\hat{\mathcal{F}}$ is (for fixed H_U) a *universal* functional of Σ and D only, from which the disconnected Green's function and the order parameter are obtained by functional derivative, see Eq. (4.23).

Given Σ and D we can compute by Eq. (4.23) the corresponding values for A and $\mathrm{G}_{\mathrm{disc}}$. On the other hand, for a specific physical system, uniquely defined by G_0^{-1}, F and H_U, the definitions of the self-energy Σ, Eq. (4.18b), and the modified order parameter D, Eq. (4.21a), provide another set of equations, which uniquely fix Σ and D via the equations

$$\begin{aligned}\hat{\mathrm{G}}_{\mathrm{disc}}[\Sigma, D] \stackrel{!}{=} (G_0^{-1} - \Sigma)^{-1} + \\ (G_0^{-1} - \Sigma)^{-1}(D - F)(\bar{D} - \bar{F})(G_0^{-1} - \Sigma)^{-1}\ ,\end{aligned} \tag{4.24a}$$

and

$$-2\bar{\mathcal{A}}[\Sigma, D] \stackrel{!}{=} -2(\bar{D} - \bar{F})(G_0^{-1} - \Sigma)^{-1}\ . \tag{4.24b}$$

As for the (original) self-energy functional approach, we seek now a functional, which becomes stationary at the exact Σ and D for specific G_0^{-1} and F, and which consists of the universal functional $\hat{\mathcal{F}}$ plus a non-universal explicit functional of the form

$$2\beta\hat{\Omega}_s[\Sigma, D, G_0^{-1}, F, H_U] = \hat{\mathcal{F}}[\Sigma, D, H_U] + \hat{\mathcal{E}}[\Sigma, D, G_0^{-1}, F] \; .$$

In order to yield the correct stationary point, the functional $\hat{\mathcal{E}}$ has to fulfill according to Eq. (4.24) the equations

$$\begin{aligned} \frac{\delta\hat{\mathcal{E}}}{\delta\Sigma} =& -(G_0^{-1}-\Sigma)^{-1} \\ & -(G_0^{-1}-\Sigma)^{-1}(D-F)(\bar{D}-\bar{F})(G_0^{-1}-\Sigma)^{-1} \; , \end{aligned} \tag{4.25a}$$

$$\frac{\delta\hat{\mathcal{E}}}{\delta D} = 2(\bar{D}-\bar{F})(G_0^{-1}-\Sigma)^{-1} \; . \tag{4.25b}$$

With these ingredients we can now express the sought-for functional $\hat{\Omega}_s$ as

$$\begin{aligned} 2\beta\hat{\Omega}_s[\Sigma,\, D, G_0^{-1}, F] =& \hat{\mathcal{F}}[\Sigma, D] + \beta\,\mathrm{Tr}\ln[(G_0^{-1}-\Sigma)\; G_\infty] \\ & + (\bar{D}-\bar{F})(G_0^{-1}-\Sigma)^{-1}(D-F) \; , \end{aligned} \tag{4.26}$$

which obviously fulfills Eq. (4.25). It remains to show that, whenever evaluated at the exact Σ and D the functional $\hat{\Omega}_s$ corresponds, possibly apart from a constant, to the thermodynamic grand potential $\widetilde{\Omega}_s$ of the system. To this end we add up all the terms used to construct the functional. At the exact values of Σ and D we have

$$\begin{aligned} 2\beta\hat{\Omega}_s\big|_{exact} &= 2\beta\widetilde{\Omega}_s + 2\bar{F}\mathcal{A} + \bar{\mathcal{A}}G_0^{-1}\mathcal{A} - \beta\,\mathrm{Tr}\left(GG_0^{-1}-\mathbb{1}\right) \\ &\quad +\beta\,\mathrm{Tr}\ln\left(G/G_\infty\right) + \beta\,\mathrm{Tr}\,\Sigma G - \bar{\mathcal{A}}\Sigma\mathcal{A} - 2\bar{D}\mathcal{A} \\ &\quad -\beta\,\mathrm{Tr}\ln\left(G/G_\infty\right) + \bar{\mathcal{A}}G^{-1}\mathcal{A} \\ &= 2\beta\widetilde{\Omega}_s - 2\underbrace{(\bar{D}-\bar{F})}_{\bar{\mathcal{A}}G^{-1}}\mathcal{A} + 2\bar{\mathcal{A}}G^{-1}\mathcal{A} \\ &= 2\beta\widetilde{\Omega}_s \end{aligned}$$

We can now proceed as in Refs. [119] and [129] and construct a reference system, which can be solved (almost) exactly. [130] The reference system is described by a Hamiltonian H', which shares the same interaction H_U as the physical system, but consists of different noninteracting Green's function G'_0 and source fields F'. The point is the following: Due to the fact that $\mathcal{F}$ is a universal functional, it cancels out from the difference between $\hat{\Omega}_s$ for the physical and the reference system, *with the same values of* Σ *and* D. In particular, this gives

$$\begin{aligned} 2\beta\hat{\Omega}_s[\Sigma, D, G_0^{-1}, F] - 2\beta\hat{\Omega}_s[\Sigma, D, G_0'^{-1}, F'] \\ = \beta \operatorname{Tr}\ln\left((G_0^{-1} - \Sigma)G_\infty\right) - \beta \operatorname{Tr}\ln\left((G_0'^{-1} - \Sigma)G_\infty\right) \\ + (\bar{D} - \bar{F})(G_0^{-1} - \Sigma)^{-1}(D - F) \\ - (\bar{D} - \bar{F}')(G_0'^{-1} - \Sigma)^{-1}(D - F')\,, \end{aligned} \tag{4.27}$$

which allows to evaluate the functional $\hat{\Omega}_s$ exactly for the physical system as well, however, in a restricted subspace of Σ and D, representable by the parametric family of reference systems. By construction, the optimal values for Σ and D for the physical system are those of the reference system for the set of optimal variational parameters.

The variational procedure then follows and generalizes Ref. [119]: First a class of exactly solvable reference systems $\hat{H}'$ with the same interaction as the physical system characterized by a continuum of single-particle parameters $\mathbf{t}'$ and source fields F' is identified. In VCA this class is obtained by dividing the original lattice into disconnected clusters with varying single-particle energies and hopping strengths. A larger subspace can be reached by adding bath sites. [120] Then the (connected) Green's function G', the order parameter $\mathcal{A}'$, and the grand potential Ω'_s of the reference system is evaluated. With the help of Dyson's equation Eq. (4.18b) the self-energy Σ', and with the help of Eq. (4.21a) D' is determined. By varying $\mathbf{t}'$ and F' the subspace of self-energies and Ds is spanned, which is accessible to the

reference system and to which these objects for the physical system are restricted. Within this subspace the functional $\hat{\Omega}_s$ can be evaluated exactly for arbitrary G_0 and F of the physical system. For the relevant case $F = 0$ we obtain [131] from Eq. (4.27)

$$\begin{aligned} 2\beta\Omega_s = 2\beta\Omega'_s &+ \beta \operatorname{Tr} \ln\left(-(G_0^{-1} - \Sigma')\right) \\ &- \beta \operatorname{Tr} \ln\left(-(G_0'^{-1} - \Sigma')\right) + \bar{D}(G_0^{-1} - \Sigma')^{-1} D \\ &- \bar{\mathcal{A}}' G'^{-1} \mathcal{A} \,, \end{aligned} \tag{4.28}$$

which is now a *function* of $\mathbf{t}'$ and F'. The infinite physical system can break the symmetry spontaneously, while in the reference systems of disconnected finite clusters, a non-vanishing order parameter can only be achieved by an additional source field F'. This explains, why a finite F' is required although $F = 0$ in the physical system. The SFA approximation consists in finding a stationary point of $\hat{\Omega}_s$ within this subspace of self-energies and D-s. This corresponds, quite generally, to finding a stationary point with respect to $\mathbf{t}'$ and F' of Eq. (4.28), i.e. to the equations

$$\frac{\partial \Omega}{\partial \mathbf{t}'} = 0 \qquad \frac{\partial \Omega}{\partial F'} = 0 \,. \tag{4.29}$$

Here, we have replaced Ω_s with $\Omega \equiv \Omega_s - \frac{1}{2} \operatorname{tr} \mathbf{t}$ which differs just by a $\mathbf{t}'$- and F'-independent constant and thus does not change the saddle-point equations. The quantity Ω is the grand potential obtained from the normal-ordered Hamiltonian (see App. 4.5.1). We also introduce the grand-potential of the normal-ordered reference system $\Omega' \equiv \Omega'_s - \frac{1}{2} \operatorname{tr} \mathbf{t}'$. This term is also present in the pseudoparticle approach, [91] where its origin is easily seen. Moreover, for τ-independent fields and Hamiltonian, the expectation values $\mathcal{A}(\tau)$ are τ-independent as well, and the Green's functions depend on the time difference only. In this way, we can rewrite

Eq. (4.28) as

$$\Omega = \Omega' - \frac{1}{2}\,\mathrm{tr}(\mathbf{t}-\mathbf{t}') - \frac{1}{2}\,\mathrm{Tr}\ln(-G) + \frac{1}{2}\,\mathrm{Tr}\ln(-G') + \frac{1}{2}\bar{\mathcal{A}}G^{-1}(\omega_n=0)\mathcal{A} - \frac{1}{2}\bar{\mathcal{A}}'G'^{-1}(\omega_n=0)\mathcal{A}' \;, \tag{4.30}$$

where $G(\omega_n) \equiv \int d\ \tau\ G(\tau,0)e^{i\tau\omega_n}$ is the Green's function in Matsubara space. The expression for Ω given in Eq. (4.30) is our main result. As can be seen, this expression is the same as Eq. (1) in Ref. [91], except for a different normalization factor, which is the number of clusters N_c. Notice that $N_c h$ in Ref. [91] is equal to $\mathbf{t}-\mathbf{t}'$ in the present paper. We thus proved that the result obtained within the pseudoparticle approach in Ref. [91] can be equivalently obtained within a more rigorous "generalized" self-energy functional approach. While the pseudoparticle approach is quite intuitive, the present self-energy approach provides a rigorous variational principle, explaining why the grand-potential Ω has to be optimized with respect to the cluster parameters $\mathbf{t}'$ and F'. In addition, as in SFA for the normal phase, it suggests more general approximations in which bath sites are used to enlarge the space of possible self-energies. [120, 132, 133]

4.3 Superfluid density

In this section we discuss the evaluation of the superfluid density ρ_s within our extended SFA/VCA theory and present results for the two-dimensional BH model.

The superfluid density is related to the response of the system to a phase-twisting field, [122,134] leading to twisted boundary conditions (BC) in one spatial direction, which we choose to be the $\mathbf{e}_x$-direction, and periodic BC in the others. The many-body wave function $|\Psi\rangle$ has to obey these BC and thus

$$\hat{T}(N_x\,\mathbf{e}_x)\,|\Psi\rangle = e^{i\Theta}\,|\Psi\rangle \;,$$

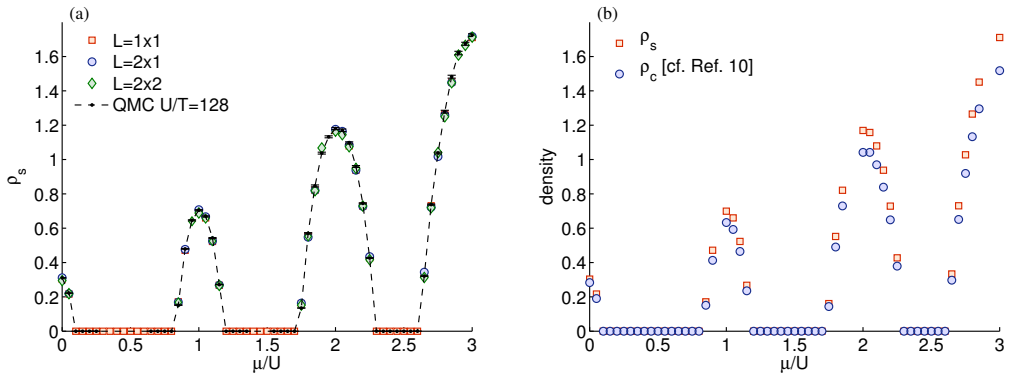

Figure 4.1: (Color online) Superfluid density ρ_s (a) evaluated for constant hopping strength $t/U = 0.02$ as a function of the chemical potential μ/U. VCA results for reference systems of size $L = 1 \times 1$, $L = 2 \times 1$, and $L = 2 \times 2$ and for essentially infinitely large physical systems are compared to QMC results for physical systems of size 32×32 and inverse temperature $U/T = 128$. Comparison of the superfluid density ρ_s and condensed density ρ_c (b) for reference systems of size $L = 1 \times 1$ and essentially infinitely large physical systems, *cf.* Ref. [91].

where the operator $\hat{T}(\mathbf{r})$ translates the particles by the vector $\mathbf{r}$, N_x is the lattice extension in $\mathbf{e}_x$-direction, and Θ is the phase twist applied to to the system. The twisted BC can be mapped by a unitary transformation onto the lattice Hamiltonian, leading to complex-valued hopping integrals. [116, 135, 136] The resulting Hamiltonian can be interpreted as a cylinder rolled up along the x-direction, which is threaded by an effective magnetic field with total flux Θ. When a particle is translated by N_x in the $\mathbf{e}_x$-direction a phase $\exp[-i\Theta]$ is picked up. [137] Due to gauge invariance, one is free to choose where the phase is collected when the particle propagates across the lattice. The usual choice is that each hopping process in the $\mathbf{e}_x$ direction, i.e., from site $\mathbf{r}' = (r_x - 1,\, r_y)$ to $\mathbf{r} = (r_x,\, r_y)$, is multiplied by a phase factor $\exp[-iA]$, where the associated vector potential is

$$A = \Theta / N_x \; . \tag{4.31}$$

When choosing the phase in that way, the reference system $\hat{H}'$ also depends on the vector potential A and the intra-cluster hopping terms become complex-valued along the $\mathbf{e}_x$-direction. For a Hamiltonian with nearest-neighbor hopping t, the superfluid density is determined from [137]

$$\rho_s = \frac{1}{t} \frac{1}{N_x\, N_y} \frac{\partial^2 \, \Omega_\Theta}{\partial \, A^2} \; , \tag{4.32}$$

where $N_x\, N_y$ is the total number of lattice sites of the physical system, and Ω_Θ is the grand potential of the physical system, subject to a phase twist Θ, as discussed above. Plugging in the vector potential of Eq. (4.31) yields

$$\rho_s = \frac{1}{t} \frac{N_x}{N_y} \frac{\partial^2 \, \Omega_\Theta}{\partial \, \Theta^2} \, . \tag{4.33}$$

In practice, the grand potential Ω_Θ is evaluated at the stationary point of Eq. (4.30), and is determined self-consistently for several values of Θ. From this data the curvature of Ω_Θ with respect to Θ is extracted from a fit. Using the curvature, the superfluid density is evaluated according to Eq. (4.33). Note that a finite cluster

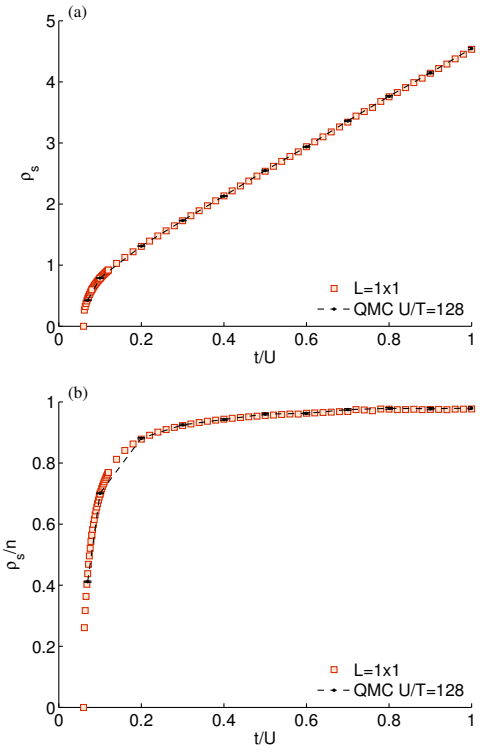

Figure 4.2: (Color online) Superfluid density ρ_s (a) and superfluid fraction ρ_s/n (b) ranging deep in the superfluid phase evaluated for constant chemical potential $\mu/U = 0.4$ as a function of the hopping strength t/U. Results obtained by means of VCA for reference systems of size $L = 1 \times 1$ and essentially infinitely large physical systems are compared to QMC results for physical systems of size 32×32 and inverse temperature $U/T = 128$.

is embedded in an essentially infinitely large system and thus the limits are taken in the correct order to obtain the superfluid density. [137]

In the following, we apply this procedure to the two-dimensional BH model [125]

$$\hat{H} = \sum_{\langle i,\, j\rangle} t_{ij}\, a_i^\dagger\, a_j + \frac{U}{2} \sum_i \hat{n}_i\,(\hat{n}_i - 1) - \mu \sum_i \hat{n}_i\ ,$$

where $a_i^\dagger$ (a_i) creates (destroys) a bosonic particle on site i, and $\hat{n}_i = a_i^\dagger\, a_i$ is the occupation number operator. The hopping integrals t_{ij} are nonzero for nearest neighbors only, as indicated by the the angle brackets. Specifically, $t_{ij} = -t$ for hopping processes along the $\mathbf{e}_y$-direction and $t_{ij} = -t \exp[i\, A\,(\mathbf{r}_i - \mathbf{r}_j)\mathbf{e}_x]$ for hopping processes along the $\mathbf{e}_x$-direction. The chemical potential, termed μ, controls the particle number and U is the repulsive on-site interaction, which subsequently will be used as unit of energy. The reference system $\hat{H}'$ consists of a cluster decomposition of the physical system $\hat{H}$ plus a $U(1)$ symmetry breaking source term

$$\begin{aligned}\hat{H}' = \sum_{\mathbf{R}} \Big[\sum_{\langle \alpha,\, \beta\rangle} t'_{\alpha\beta} a^\dagger_{\alpha,\mathbf{R}}\, a_{\beta,\mathbf{R}} + \frac{U}{2} \sum_\alpha \hat{n}_{\alpha,\mathbf{R}}\,(\hat{n}_{\alpha,\mathbf{R}} - 1) \\ - \mu' \sum_\alpha \hat{n}_{\alpha,\mathbf{R}} - \sum_\alpha (a^\dagger_{\alpha,\mathbf{R}}\, f_\alpha + f^*_\alpha\, a_{\alpha,\mathbf{R}})\Big]\ ,\end{aligned}$$

where the lattice site indices i have been decomposed into an index $\mathbf{R}$, that specifies the cluster and into an index α, that specifies the lattice sites within a cluster. [91,138] Analogously to the physical system, the hoping integrals are $t'_{\alpha\beta} = -t'$ and $t'_{\alpha\beta} = -t' \exp[i\, A\,(\mathbf{r}_{\mathbf{R}\alpha} - \mathbf{r}_{\mathbf{R}\beta})\mathbf{e}_x]$ for nearest-neighbor hopping processes along the $\mathbf{e}_y$- and the $\mathbf{e}_x$-direction, respectively, and zero otherwise. In our calculation, we use the chemical potential μ' and the source coupling strength f_α of the reference system as variational parameters in the optimization prescription. Since the reference system is complex valued, the source coupling strength f_α is complex valued too, i.e., $f_\alpha = |f_\alpha| \exp[\phi_\alpha]$. Thus, in general, $2L$ variational parameters

have to be considered, where L is the number of cluster sites. However, for different cluster sites α the source coupling strengths f_α are interrelated, as can be seen from mean field arguments, leading effectively to two variational parameters $|f|$ and ϕ, which we use—in addition to the chemical potential μ'—to treat complex valued reference systems.

In Fig. 4.1 we present the superfluid density ρ_s for different sizes of the reference system ranging from $L = 1 \times 1$, over $L = 2 \times 1$, to $L = 2 \times 2$ and essentially infinitely large physical systems. For the largest cluster we restrict the variational search space to real valued order parameters, i.e., we set $\phi_\alpha = 0$. Figure 4.1 (a) demonstrates that this choice leads to comparable results as obtained with the full variational space. Yet, for the restricted variational space the computational effort as well as the numerical complexity is reduced, since the reference system remains real valued. Figure 4.1 (a) shows the superfluid density ρ_s, as a function of the chemical potential μ/U evaluated for fixed hopping strength $t/U = 0.02$. The chemical potential ranges from $\mu/U = 0$ to $\mu/U = 3$. As the hopping strength is small, three regions with $\rho_s = 0$ are present, corresponding to the Mott insulating phase. In between these regions, we observe a finite superfluid density ρ_s indicating the occurrence of the superfluid phase. In addition to the VCA results, we show QMC results with errorbars (barely visible) for physical systems of size 32×32 and inverse temperature $U/T = 128$. The QMC calculations were performed with the ALPS library [139] and the ALPS applications. [140] Particularly, we use the stochastic series expansion representation of the partition function with directed loop updates, [141–143] where the superfluid density is evaluated via the winding number. [123,124] The superfluid density ρ_s obtained from VCA agrees remarkable well with the QMC results. Furthermore, VCA results are almost independent of the size L of the reference system, signaling convergence to the correct results even for $L = 1 \times 1$ site clusters. The superfluid density ρ_s is compared to the

condensate density $\rho_c = \langle a_i \rangle$ in Fig. 4.1 (b), *cf.* Ref. [91]. It can be observed that the superfluid density is always larger than the density of the Bose-Einstein condensate. However, the difference between the two densities is rather small, since a very dilute Bose gas is investigated.

In Fig. 4.2 we evaluate (a) the superfluid density ρ_s and (b) the superfluid fraction ρ_s/n (n is the particle density) for fixed chemical potential $\mu/U = 0.4$ as a function of the hopping strength t/U. The hopping strength ranges from $t/U = 0$ to $t/U = 1$, which is already very deep in the superfluid phase. For $\mu/U = 0.4$ the phase boundary between the Mott and the superfluid phase is located at $t/U \approx 0.06$. In the superfluid phase close to the phase boundary the superfluid density rises quickly from zero developing an almost linear behavior for $t/U \gtrsim 0.2$. In the latter parameter regime the superfluid fraction is larger than 90% signaling that already a very large amount of the lattice bosons is superfluid. As emphasized in Ref. [144], a relatively sharp crossover from a strongly-correlated superfluid, characterized by a superfluid fraction which is well below 1, to a weakly-correlated superfluid, where the superfluid fraction is almost 1, can be observed, see Fig. 4.2 (b). In addition to the VCA results evaluated for reference systems of size $L = 1 \times 1$ and essentially infinitely large physical systems, we show QMC results for physical systems of size 32×32 and inverse temperature $U/T = 128$, which again exhibit perfect agreement.

In Fig. 4.3 we focus on the quantum critical region close to the tip of the first Mott lobe, which is the most challenging one. In particular, we evaluate the particle density n, the condenstate density ρ_c, and superfluid density ρ_s. In the first row we show results for fixed chemical potential $\mu/U = 0.4$ as a function of the hopping strength t/U, whereas in the second row we keep hopping strength fixed at $t/U = 0.05$ and vary the chemical potential μ/U. We compare VCA results with QMC and mean-field (MF). The most important observation is that

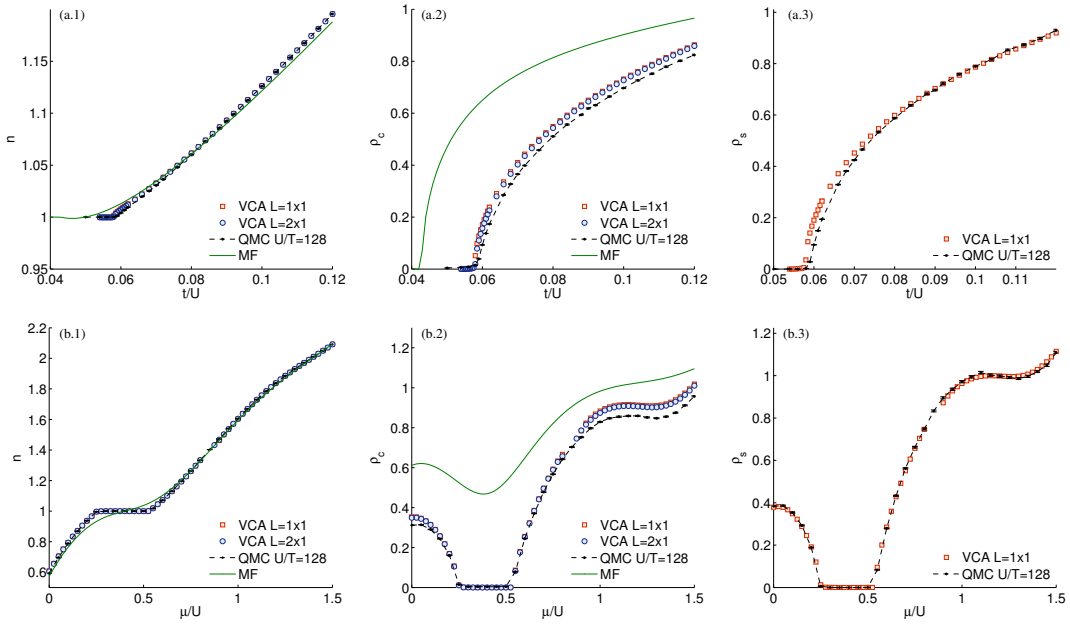

Figure 4.3: (Color online) Particle density n (left), condensate density ρ_c (middle), and superfluid density ρ_s (right) evaluated around the quantum critical region close to the tip of the first Mott lobe. Comparison of the data obtained by means of VCA (for essentially infinitely large physical systems and reference systems as stated in the legends), QMC (for physical systems of size 32×32 and inverse temperatures $U/T = 128$), and mean-field. The first row (a.$*$) shows results for fixed chemical potential $\mu/U = 0.4$ as a function of the hopping strength t/U, whereas the second row (b.$*$) shows results for fixed hopping strength $t/U = 0.05$ as a function of the chemical potential μ/U.

MF is far off QMC and VCA. For $\mu/U = 0.4$ MF predicts the phase transition to be at a much smaller value of t/U than QMC and VCA. This leads to significant deviations in both the density and condensate density as compared to QMC and VCA. For fixed $t/U = 0.05$ MF does not enter the Mott region and thus does not predict a plateau in the density. For both investigated situations (fixed μ/U and fixed t/U) the results obtained by means of VCA and QMC agree quite well. For the QMC simulations we used lattices of size 32×32 and inverse temperatures of $U/T = 128$. The VCA results are obtained at zero temperature for clusters of size 1×1 and 2×1, respectively, and essentially infinitely large physical systems. In this challenging regime small differences between VCA and QMC are observable for the condensate density. For the reference system sizes considered here, results are almost identical. Larger reference systems might still reduce the difference between VCA and QMC. However, close to the phase transition finite size and finite temperature effects might still be important for the QMC results, and thus a proper finite size scaling of these data might also reduce the discrepancy between the two approaches. Note that for fixed hopping $t/U = 0.05$ there is a very small region at $\mu/U \approx 0.85$, where it is difficult to numerically determine the stationary point of the grand potential. Such a region is also present between the first and the second and between the second and the third Mott lobe in Fig. 4.1. However, there it is barely visible since the spacing between two consecutive μ datapoints is larger than this gap. This failure appears to be related to the fact that two solutions adiabatically connected to two sectors with different particle numbers, i. e. the two neighboring Mott regions, meet and try to avoid each other. However, we want to emphasize that this affects only a tiny region of the phase diagram. When keeping the chemical potential fixed at $\mu/U = 0.4$ solutions can be easily found for all values of the hopping strength.

Finally, we want to emphasize that the VCA results are obtained with very mod-

est computational effort and that excellent agreement with QMC can be observed, even for very small reference systems.

4.4 Conclusions

In the present work, we extend the self-energy functional approach to the $U(1)$ symmetry broken, superfluid phase of correlated lattice bosons. A crucial point of this extension is the identification of a quantity, termed D, which is the companion of the self-energy Σ in the superfluid phase. We also identify the appropriate (nonuniversal) functional $\hat{\Omega}_s$ which is stationary at the physical values of the self-energy Σ and of D. In analogy to the self-energy, which is the difference of the interacting and non-interacting Green's function, the quantity D is related to the difference of the order parameter of the interacting and non-interacting systems. Thus, D is zero in the normal phase and for $U = 0$. From these relations also follows that both Σ as well as D vanish in the non-interacting case. Importantly, when the functional $\hat{\Omega}_s$ is evaluated at the exact values of Σ and D it corresponds to the grand potential of the physical Hamiltonian. To evaluate the functional, we proceed as in the original self-energy functional approach, [119] and introduce a reference system, which is a cluster decomposition of the physical system. Importantly, the reference system shares its two-particle interaction with the physical system, and can be exactly solved by numerical methods. By comparison of the functionals, the universal part of $\hat{\Omega}_s$, denoted as $\hat{\mathcal{F}}$, can be eliminated, which allows to evaluate $\hat{\Omega}_s$ exactly on the subspace of Σ and D, spanned by the possible sets of reference systems. The results presented are shown to be equivalent to the ones obtained by a more heuristic method, the pseudoparticle approach introduced in Ref. [91], and thus provide rigorous variational grounds for that approach. In addition, the extended self-energy functional approach introduced here allows to

envision more general reference systems, in which bath sites are incorporated to enlarge the space of possible self-energies Σ, and possibly bridge over to (Cluster) Dynamical Mean Field Theory (DMFT). [93, 119] For future research it would be interesting to verify whether in the limit of an infinite number of bath sites and for a single correlated site as a reference system, our superfluid SFA becomes equivalent to DMFT for superfluid bosons, [145, 146] as it is the case in the normal phase. [119] For a finite number of bath sites this is certainly not the case, since the order parameter in the reference system differs from the physical one.

We also presented how the superfluid density can be evaluated by means of this extended variational cluster approach. To this end we applied a phase twisting field to the system. We evaluated the superfluid density for the two-dimensional Bose-Hubbard model and compared the extended variational cluster approach results with unbiased quantum Monte Carlo results, yielding remarkable agreement. We want to emphasize that the extended self-energy functional approach is not only applicable to the Bose-Hubbard model but to a large class of lattice models, which exhibit a condensed phase. This includes experimentally interesting systems such as disordered bosons, multicomponent systems (Bose-Bose mixtures or Bose-Fermi mixtures) and light matter systems. [45,147] In principle, the method cannot treat long-range interactions, such as dipolar ones, exactly. [148,149] However, the long-range part can be incorporated on a mean-field level. [150] Basically, the present approach can be applied to systems with broken translational invariance as well, and, for example, can consider the effect of a confining magnetic trap. However, in this case one has to abandon the Fourier transform in the cluster vectors and work in real space and thus work with larger matrices and a larger number of variational parameters. A convenient, numerically less expensive alternative, is to adopt the so-called local density approximation. [151]

4.5 Appendix

4.5.1 Notation and conventions

Matrix notation

General: In order to simplify our notation we omit time arguments, whenever this does not cause ambiguities. Therefore, two-point functions such as Green's functions, self-energies, etc. are interpreted as matrices in Nambu, orbital, and τ space. One-point objects such as $\mathcal{A}$ ($\bar{\mathcal{A}}$) are interpreted as column (row) vectors in the same space. Matrix-matrix and vector-matrix products are understood throughout, whereby internal τ variables are considered to be integrated over. In addition, the transposing operator "^{T}" also acts on time variables. Traces Tr contain an integral over τ and a trace tr over orbital indices, i.e., $\mathrm{Tr}\, M \equiv \mathrm{tr} \int_0^\beta d\tau M(\tau, \tau + 0^+)$, where the 0^+ leads to the well known convergence factor $e^{i\omega_n 0^+}$ in Matsubara space.

(Functional) derivatives with respect to matrices are defined "transposed":

$$\left(\frac{\delta \hat{X}}{\delta M}\right)_{ij} (\tau, \tau') \equiv \frac{\delta \hat{X}}{\delta M_{ji}(\tau', \tau)} \; .$$

Finally, there are two types of products between row (in the form $\bar{v}$) and column (u) vectors, depending on the order: On the one hand the product $\bar{v}u$ produces a scalar (all indices are summed/integrated over). On the other hand, inverting the order, as in $u\bar{v}$ gives a matrix, as indices are "external" and, thus, not summed over.

Trace in τ and in Matsubara space: In τ space we have

$$\mathrm{Tr}\, M = \beta^{-1} \mathrm{tr} \int_0^\beta d\tau \; M(\tau, \tau + 0^+) \; .$$

The transformation of $M(\tau,\tau')$ to Matsubara space is defined as

$$M(\tau,\tau') \equiv \beta^{-1} \sum_{n,n'} M(\omega_n,\omega'_n) e^{-i\omega_n\tau + i\omega'_n\tau'} \ .$$

The inverse transformation reads

$$M(\omega_n,\omega'_n) = \beta^{-1} \int d\tau d\tau' M(\tau,\tau') e^{i\omega_n\tau - i\omega'_n\tau'} \ .$$

Combining the equations above, the trace becomes

$$\begin{aligned} \mathrm{Tr}\, M &= \mathrm{tr} \int_0^\beta d\tau \beta^{-2} \sum_{n,n'} M(\omega_n,\omega'_n) e^{-i(\omega_n-\omega'_n)\tau + i\omega'_n 0^+} \\ &= \beta^{-1} \sum_n \mathrm{tr} M(\omega_n,\omega_n) e^{i\omega_n 0^+} \ . \end{aligned}$$

Logarithm: There are some subtle points concerning logarithms of two-point functions. Although these issues are immaterial for the final result, we prefer to specify them in detail.

The logarithm of G considered as a matrix in the continuum variable τ is defined up to an infinite constant which depends on the the discretization step δ (see below). In addition, the trace of the logarithm carried out in Matsubara space diverges as well (despite the convergence factor $e^{i\omega_n 0^+}$). The usual result presented in the literature (see, for instance Ref. [152]) implicitly assumes that an infinite constant has been subtracted. In order to avoid these undetermined infinite terms, we subtract them explicitly at the outset with the help of the "infinite energy" Green's function

$$\begin{aligned} G_\infty(\tau,\tau') &= \beta^{-1} \sum_n G_\infty(\omega_n) e^{-i\omega_n(\tau-\tau')} \\ G_\infty(\omega_n) &= \mathbb{1} \frac{1}{i\omega_n - E} \ , \end{aligned}$$

where it is understood that the $E \to +\infty$ limit is taken at the end of the calculation. This choice guarantees, for example, that $\mathrm{Tr} \ln G/G_\infty$, where G is the Green's

function in normal (i.e. not Nambu) notation, vanishes in the limit $\mu \to -\infty$, where μ is the chemical potential.

The Fourier transform defined in App. 4.5.1 allows to define the logarithm of G in τ space, apart from an infinite multiplicative constant, which originates from the fact that the Fourier transformation is not and cannot be normalized in the continuum limit. In particular,

$$\begin{aligned}[\ln(-G)](\tau,\tau') &= \beta^{-1}\sum_{n,n'}[\ln(-G)](\omega_n,\omega_n')e^{-i\omega_n\tau+i\omega_n'\tau'} \\ &= \beta^{-1}\sum_{n}\ln\left[-G(\omega_n)\right]e^{-i\omega_n(\tau-\tau')}\ ,\end{aligned}$$

Symmetry of Green's functions and other two-point functions

The action in Eq. (4.5) is invariant under the transformation $G_0 \to (\mathcal{T}G_0^T\mathcal{T})$, where the transposing operator "^{T}" also acts on time variables and $\mathcal{T}$ is defined in Eq. (4.8). This is due to the fact that

$$\begin{aligned}\bar{A}(\tau')G_0^{-1}(\tau',\tau)A(\tau) &= A(\tau')^T\mathcal{T}G_0^{-1}(\tau',\tau)\mathcal{T}\bar{A}(\tau)^T \\ &= \bar{A}(\tau)(\mathcal{T}G_0^{-1}(\tau',\tau)^T\mathcal{T})A(\tau')\ .\end{aligned}$$

Therefore, we choose G_0 to obey the symmetry

$$G_0 = (\mathcal{T}G_0^T\mathcal{T})\ . \tag{4.34}$$

The same symmetry is obeyed by other two-point functions, such as the interacting Green's function G, the self-energy Σ, and their inverse.

In principle, this redundancy renders relations such as Eq. (4.15) non invertible. In order to avoid this, we adopt the convention that functional inversions are carried out within the subspace of two-point functions obeying the relation Eq. (4.34). In addition, we adopt the following convention for functional derivatives of an ar-

bitrary functional $\hat{\Xi}$ with respect to a two-point function X:

$$\frac{\delta\hat{\Xi}}{\delta X} \to \frac{1}{2}\left(\frac{\delta\hat{\Xi}}{\delta X} + \frac{\delta\hat{\Xi}}{\delta\mathcal{T}X^T\mathcal{T}}\right) .$$

Continuum limit of the functional integral

In principle, the expression Eq. (4.10) should be understood such that adjoint fields $\bar{a}$ are evaluated at a later imaginary time $\tau + \delta$, whereby δ is the width of the discretization mesh of the interval $(0, \beta)$. The continuum limit $\delta \to 0$ should be taken after having carried out the functional integration, see, e.g. Ref. [153]. Taking this limit at the outset amounts to neglecting the so-called "contribution from infinity". [154, 155] This can be achieved by effectively replacing the normal-ordered Hamiltonian with a "symmetrically ordered" one, which is suitably symmetrized among possible permutation of creation and annihilation operators. [156] In particular, for the noninteracting part, this amounts to replacing the operator expression $a^\dagger a$ by $\frac{1}{2}(a^\dagger a + aa^\dagger) = a^\dagger a + \frac{1}{2}$. Therefore, we should keep in mind that the grand-potential $\widetilde{\Omega}_s$ corresponds to such a symmetrized Hamiltonian.

5 Acknowledgements

For the work presented in Chapter 1, we are grateful to E. G. Dalla Torre for insightful discussions about the Luttinger liquid analysis. M.K. wants to thank W. von der Linden and E. Arrigoni for fruitful discussions. The authors acknowledge support from Harvard-MIT CUA, the NSF Grants No. DMR-07-05472 and No. DMR-07-57145, the DARPA OLE program, AFOSR Quantum Simulation MURI, AFOSR MURI on Ultracold Molecules, the Austrian Science Fund (FWF) under Project No. P18551-N16 (M.K.) and within the SFB ViCoM (F41) (M.G.), as well as the Austrian Marshall Plan Foundation (M.K.). Calculations have been partly performed on the iCluster of Graz University of Technology.

For Chapter 2 and 3 we made use of the ALPS library and the ALPS applications. [139, 140] We acknowledge financial support from the Austrian Science Fund (FWF) under the doctoral program "Numerical Simulations in Technical Sciences" Grant No. W1208-N18 (M.K.) and under Project No. P18551-N16 and P21289-N16 (M.K., E.A.).

I would like to thank W. von der Linden and E. Arrigoni from Graz University of Technology and E. Demler, E. Berg, and D. A. Abanin from Harvard University for enlightening discussions and for guiding me through this interesting direction of manybody physics.

Bibliography

[1] Knap, M. Doctoral thesis (2012).

[2] Knap, M., Berg, E., Ganahl, M. & Demler, E. Clustered wigner crystal phases of cold polar molecules in arrays of one-dimensional tubes. *arXiv:1112.5662* (2011).

[3] Knap, M., von der Linden, W. & Arrigoni, E. Nonequilibrium steady state for strongly-correlated many-body systems: Variational cluster approach. *Phys. Rev. B* **84**, 115145 (2011).

[4] Arrigoni, E., Knap, M. & von der Linden, W. Extended self-energy functional approach for strongly-correlated lattice bosons in the superfluid phase. *Phys. Rev. B* **84**, 014535 (2011).

[5] Ng, K. & Vanderbilt, D. Stability of periodic domain structures in a two-dimensional dipolar model. *Phys. Rev. B* **52**, 2177 (1995).

[6] Marchenko, V. I. On the domain structure of two-dimensional ferromagnets. *Zh. Eksp. Teor. Fiz.* **90**, 2241 (1986).

[7] Rosenweig, R. E. *Ferrohydrodynamics* (Cambridge University Press, 1985).

[8] Spivak, B. & Kivelson, S. A. Phases intermediate between a two-dimensional electron liquid and wigner crystal. *Phys. Rev. B* **70**, 155114 (2004).

[9] Spivak, B., Kravchenko, S. V., Kivelson, S. A. & Gao, X. P. A. Colloquium: Transport in strongly correlated two dimensional electron fluids. *Rev. Mod. Phys.* **82**, 1743–1766 (2010).

[10] Koulakov, A. A., Fogler, M. M. & Shklovskii, B. I. Charge density wave in Two-Dimensional electron liquid in weak magnetic field. *Phys. Rev. Lett.* **76**, 499–502 (1996).

[11] Moessner, R. & Chalker, J. T. Exact results for interacting electrons in high landau levels. *Phys. Rev. B* **54**, 5006–5015 (1996).

[12] Fogler, M. M. Stripe and bubble phases in quantum hall systems. In *High Magnetic Fields: Applications in Condensed Matter Physics and Spectroscopy*, 98–138 (Springer, Berlin, 2002), 1 edn.

[13] Eisenstein, J. P., Cooper, K. B., Pfeiffer, L. N. & West, K. W. Insulating and fractional quantum hall states in the first excited landau level. *Phys. Rev. Lett.* **88**, 076801 (2002).

[14] Santos, L., Shlyapnikov, G. V., Zoller, P. & Lewenstein, M. Bose-Einstein condensation in trapped dipolar gases. *Phys. Rev. Lett.* **85**, 1791–1794 (2000).

[15] Baranov, M. A., Marâenko, M. S., Rychkov, V. S. & Shlyapnikov, G. V. Superfluid pairing in a polarized dipolar fermi gas. *Phys. Rev. A* **66**, 013606 (2002).

[16] Doyle, J., Friedrich, B., Krems, R. V. & Masnou-Seeuws, F. Editorial: Quo vadis, cold molecules? *Eur. Phys. J. D* **31**, 149–164 (2004).

[17] Baranov, M. Theoretical progress in many-body physics with ultracold dipolar gases. *Phys. Rep.* **464**, 71–111 (2008).

[18] Carr, L. D., DeMille, D., Krems, R. V. & Ye, J. Cold and ultracold molecules: science, technology and applications. *New J. Phys.* **11**, 055049 (2009).

[19] Lahaye, T., Menotti, C., Santos, L., Lewenstein, M. & Pfau, T. The physics of dipolar bosonic quantum gases. *Rep. Prog. Phys.* **72**, 126401 (2009).

[20] Wunsch, B. *et al.* Few-Body bound states in dipolar gases and their detection. *Phys. Rev. Lett.* **107**, 073201 (2011).

[21] Dalmonte, M., Zoller, P. & Pupillo, G. Trimer liquids and crystals of polar molecules in coupled wires. *Phys. Rev. Lett.* **107**, 163202 (2011).

[22] Chotia, A. *et al.* Long-lived dipolar molecules and feshbach molecules in a 3D optical lattice. *arXiv:1110.4420* (2011).

[23] Giamarchi, T. *Quantum Physics in One Dimension* (Oxford University Press, USA, 2004).

[24] White, S. R. Density matrix formulation for quantum renormalization groups. *Phys. Rev. Lett.* **69**, 2863 (1992).

[25] Schollwöck, U. The density-matrix renormalization group. *Rev. Mod. Phys.* **77**, 259 (2005).

[26] Ni, K. *et al.* A high Phase-Space-Density gas of polar molecules. *Science* **322**, 231 –235 (2008).

[27] Debatin, M. *et al.* Molecular spectroscopy for ground-state transfer of ultracold RbCs molecules. *arXiv:1106.0129* (2011).

[28] Park, J. W. *et al.* Quantum degenerate Bose-Fermi mixture of chemically different atomic species with widely tunable interactions. *arXiv:1110.4552* (2011).

[29] Haimberger, C., Kleinert, J., Dulieu, O. & Bigelow, N. P. Processes in the formation of ultracold NaCs. *J. Phys. B: At. Mol. Opt. Phys.* **39**, S957–S963 (2006).

[30] Deiglmayr, J. *et al.* Formation of ultracold dipolar molecules in the lowest vibrational levels by photoassociation. *Faraday Discuss.* **142**, 335–349 (2009).

[31] Müller, C. A., Jonckheere, T., Miniatura, C. & Delande, D. Weak localization of light by cold atoms: The impact of quantum internal structure. *Phys. Rev. A* **64**, 053804 (2001).

[32] Altman, E., Demler, E. & Lukin, M. D. Probing many-body states of ultracold atoms via noise correlations. *Phys. Rev. A* **70**, 013603 (2004).

[33] Zinner, N. T. *et al.* Few-body bound complexes in one-dimensional dipolar gases and nondestructive optical detection. *Phys. Rev. A* **84**, 063606 (2011).

[34] Stöferle, T., Moritz, H., Schori, C., Köhl, M. & Esslinger, T. Transition from a strongly interacting 1D superfluid to a mott insulator. *Phys. Rev. Lett.* **92**, 130403 (2004).

[35] Regal, C. A. & Jin, D. S. Measurement of positive and negative scattering lengths in a fermi gas of atoms. *Phys. Rev. Lett.* **90**, 230404 (2003).

[36] Gupta, S. *et al.* Radio-Frequency spectroscopy of ultracold fermions. *Science* **300**, 1723 –1726 (2003).

[37] Regal, C. A., Ticknor, C., Bohn, J. L. & Jin, D. S. Creation of ultracold molecules from a fermi gas of atoms. *Nature* **424**, 47–50 (2003).

[38] Ewald, P. P. Die berechnung optischer und elektrostatischer gitterpotentiale. *Ann. Phys.* **369**, 253–287 (1921).

[39] Essmann, U. *et al.* A smooth particle mesh ewald method. *J. Chem. Phys.* **103**, 8577 (1995).

[40] Grzybowski, A., Gwóźdź, E. & Bródka, A. Ewald summation of electrostatic interactions in molecular dynamics of a three-dimensional system with periodicity in two directions. *Phys. Rev. B* **61**, 6706–6712 (2000).

[41] Kollath, C., Meyer, J. S. & Giamarchi, T. Dipolar bosons in a planar array of One-Dimensional tubes. *Phys. Rev. Lett.* **100**, 130403 (2008).

[42] Jaksch, D., Bruder, C., Cirac, J. I., Gardiner, C. W. & Zoller, P. Cold bosonic atoms in optical lattices. *Phys. Rev. Lett.* **81**, 3108 (1998).

[43] Greiner, M., Mandel, O., Esslinger, T., Hänsch, T. W. & Bloch, I. Quantum phase transition from a superfluid to a mott insulator in a gas of ultracold atoms. *Nature (London)* **415**, 39–44 (2002).

[44] Bloch, I., Dalibard, J. & Zwerger, W. Many-body physics with ultracold gases. *Rev. Mod. Phys.* **80**, 885–80 (2008).

[45] Hartmann, M., Brandão, F. G. & Plenio, M. B. Quantum many-body phenomena in coupled cavity arrays. *Laser Photonics Rev.* **2**, 527–556 (2008).

[46] Tomadin, A. & Fazio, R. Many – body phenomena in qed – cavity arrays. *J. Opt. Soc. Am. B* **27**, A130 (2010).

[47] Park, H. *et al.* Nanomechanical oscillations in a single-c60 transistor. *Nature* **407**, 57 (2000).

[48] Paaske, J. & Flensberg, K. Vibrational sidebands and the kondo effect in molecular transistors. *Phys. Rev. Lett.* **94**, 176801 (2005).

[49] Zutic, I., Fabian, J. & Sarma, S. D. Spintronics: Fundamentals and applications. *Rev. Mod. Phys.* **76**, 323 (2004).

[50] Fabian, J., Matos-Abiague, A., Ertler, C., Stano, P. & Zutic, I. Semiconductor spintronics. *Acta Physica Slovaca* **57**, 565 (2007).

[51] Slobodskyy, A. *et al.* Voltage-controlled spin selection in a magnetic resonant tunneling diode. *Phys. Rev. Lett.* **90**, 246601 (2003).

[52] Bonilla, L. L. & Grahn, H. T. Non-linear dynamics of semiconductor superlattices. *Rep. Prog. Phys.* **68**, 577 (2005).

[53] Jungwirth, T., Sinova, J., Masek, J., Kucera, J. & MacDonald, A. H. Theory of ferromagnetic (III,Mn)V semiconductors. *Rev. Mod. Phys.* **78**, 809 (2006).

[54] Ertler, C., Pötz, W. & Fabian, J. Proposal for a ferromagnetic multiwell spin oscillator. *Appl. Phys. Lett.* **97**, 042104 (2010).

[55] Ertler, C., Senekowitsch, P., Fabian, J. & Pötz, W. Self-consistent study of transport in mn-doped semiconductor heterostructures. In *Computational Electronics (IWCE), 2010 14th International Workshop on*, 1–4 (2010).

[56] Sokolowski-Tinten, K. *et al.* Femtosecond x-ray measurement of coherent lattice vibrations near the lindemann stability limit. *Nature* **422**, 287–289 (2003).

[57] Haug, H. & Jauho, A.-P. *Quantum Kinetics in Transport and Optics of Semiconductors* (Springer, Heidelberg, 1998).

[58] Rammer, J. & Smith, H. Quantum field-theoretical methods in transport theory of metals. *Rev. Mod. Phys.* **58**, 323–359 (1986).

[59] Meir, Y. & Wingreen, N. S. Landauer formula for the current through an interacting electron region. *Phys. Rev. Lett.* **68**, 2512–2515 (1992).

[60] Meir, Y., Wingreen, N. S. & Lee, P. A. Low-temperature transport through a quantum dot: The anderson model out of equilibrium. *Phys. Rev. Lett.* **70**, 2601–2604 (1993).

[61] Ryndyk, D. A., Gutierrez, R., Song, B. & Cuniberti, G. Green function techniques in the treatment of quantum transport at the molecular scale. In Castleman, A. W. *et al.* (eds.) *Energy Transfer Dynamics in Biomaterial Systems*, vol. 93 of *Springer Series in Chemical Physics*, 213–335 (Springer Berlin Heidelberg, 2009).

[62] Schoeller, H. A perturbative nonequilibrium renormalization group method for dissipative quantum mechanics. *Eur. Phys. J. Special Topics* **168**, 179–266 (2009).

[63] Diehl, S. *et al.* Quantum states and phases in driven open quantum systems with cold atoms. *Nat. Phys.* **4**, 878 – 883 (2008).

[64] Kraus, B. *et al.* Preparation of entangled states by quantum markov processes. *Phys. Rev. A* **78**, 042307 (2008).

[65] Diehl, S., Tomadin, A., Micheli, A., Fazio, R. & Zoller, P. Dynamical phase transitions and instabilities in open atomic many-body systems. *Phys. Rev. Lett.* **105**, 015702 (2010).

[66] Pichler, H., Daley, A. J. & Zoller, P. Nonequilibrium dynamics of bosonic atoms in optical lattices: Decoherence of many-body states due to spontaneous emission. *Phys. Rev. A* **82**, 063605 (2010).

[67] Tomadin, A., Diehl, S. & Zoller, P. Nonequilibrium phase diagram of a driven and dissipative many-body system. *Phys. Rev. A* **83**, 013611 (2011).

[68] Barmettler, P. & Kollath, C. Dynamical response of a bosonic quantum gas to local one-body losses. *arXiv:1012.0422* (2010).

[69] Dalla Torre, E. G., Demler, E., Giamarchi, T. & Altman, E. Quantum critical states and phase transitions in the presence of non-equilibrium noise. *Nat. Phys.* **6**, 806–810 (2010).

[70] White, S. R. & Feiguin, A. E. Real-time evolution using the density matrix renormalization group. *Phys. Rev. Lett.* **93**, 076401 (2004).

[71] Daley, A. J., Kollath, C., Schollwöck, U. & Vidal, G. Time-dependent density-matrix renormalization-group using adaptive effective hilbert spaces. *J. Stat. Mech.* **2004**, P04005 (2004).

[72] Prosen, T. & Žnidarič, M. Matrix product simulations of non-equilibrium steady states of quantum spin chains. *J. Stat. Mech.* **2009**, P02035 (2009).

[73] Benenti, G., Casati, G., Prosen, T., Rossini, D. & Žnidarič, M. Charge and spin transport in strongly correlated one-dimensional quantum systems driven far from equilibrium. *Phys. Rev. B* **80**, 035110 (2009).

[74] Perez-Garcia, D., Verstraete, F., Wolf, M. M. & Cirac, J. I. Matrix product state representations. *Quant. Inf. Comp.* **7**, 401 (2007).

[75] Werner, P., Oka, T. & Millis, A. J. Diagrammatic monte carlo simulation of nonequilibrium systems. *Phys. Rev. B* **79**, 035320 (2009).

[76] Anders, F. B. & Schiller, A. Spin precession and real-time dynamics in the kondo model:time-dependent numerical renormalization-group study. *Phys. Rev. B* **74**, 245113 (2006).

[77] Jakobs, S. G., Meden, V. & Schoeller, H. Nonequilibrium functional renormalization group for interacting quantum systems. *Phys. Rev. Lett.* **99**, 150603 (2007).

[78] Freericks, J. K., Turkowski, V. M. & Zlatic, V. Nonequilibrium dynamical Mean-Field theory. *Phys. Rev. Lett.* **97**, 266408 (2006).

[79] Joura, A. V., Freericks, J. K. & Pruschke, T. Steady-state nonequilibrium density of states of driven strongly correlated lattice models in infinite dimensions. *Phys. Rev. Lett.* **101**, 196401 (2008).

[80] Eckstein, M., Kollar, M. & Werner, P. Thermalization after an interaction quench in the hubbard model. *Phys. Rev. Lett.* **103**, 056403 (2009).

[81] Aron, C., Kotliar, G. & Weber, C. Dimensional crossover driven by electric field (2011). ArXiv:1105.5387.

[82] Mehta, P. & Andrei, N. Nonequilibrium transport in quantum impurity models: The bethe ansatz for open systems. *Phys. Rev. Lett.* **96**, 216802 (2006).

[83] Gritsev, V., Rostunov, T. & Demler, E. Exact methods in the analysis of the non-equilibrium dynamics of integrable models: application to the study of correlation functions for non-equilibrium 1D bose gas. *J. Stat. Mech.* **2010**, P05012 (2010).

[84] Jung, C. *et al.* Dual-Fermion approach to non-equilibrium strongly correlated problems. *arXiv:1011.3264* (2010).

[85] Balzer, M. & Potthoff, M. Nonequilibrium cluster perturbation theory. *Phys. Rev. B* **83**, 195132 (2011).

[86] Myöhänen, P., Stan, A., Stefanucci, G. & van Leeuwen, R. Kadanoff-Baym approach to quantum transport through interacting nanoscale systems: From the transient to the steady-state regime. *Phys. Rev. B* **80** (2009).

[87] Brandbyge, M., Mozos, J.-L., Ordejón, P., Taylor, J. & Stokbro, K. Density-functional method for nonequilibrium electron transport. *Phys. Rev. B* **65**, 165401 (2002).

[88] Fürst, J., Brandbyge, M., Jauho, A. & Stokbro, K. Ab initio study of spin-dependent transport in carbon nanotubes with iron and vanadium adatoms. *Phys. Rev. B* **78** (2008).

[89] Markussen, T., Jauho, A. & Brandbyge, M. Electron and phonon transport in silicon nanowires: Atomistic approach to thermoelectric properties. *Phys. Rev. B* **79** (2009).

[90] Dahnken, C., Aichhorn, M., Hanke, W., Arrigoni, E. & Potthoff, M. Variational cluster approach to spontaneous symmetry breaking:
the itinerant antiferromagnet in two dimensions. *Phys. Rev. B* **70**, 245110 (2004).

[91] Knap, M., Arrigoni, E. & von der Linden, W. Variational cluster approach for strongly – correlated lattice bosons in the superfluid phase. *Phys. Rev. B* **83**, 134507 (2011).

[92] Metzner, W. & Vollhardt, D. *Phys. Rev. Lett.* **62**, 324 (1989).

[93] Georges, A., Kotliar, G., Krauth, W. & Rozenberg, M. J. The local impurity self consistent approximation (LISA) to strongly correlated fermion systems and the limit of infinite dimensions. *Rev. Mod. Phys.* **68**, 13 (1996).

[94] Kotliar, G., Savrasov, S. Y., Pálsson, G. & Biroli, G. Cellular dynamical mean field approach to strongly correlated systems. *Phys. Rev. Lett.* **87**, 186401 (2001).

[95] Potthoff, M. Self – energy – functional approach to systems of correlated electrons. *Eur. Phys. J. B* **32**, 429 (2003).

[96] Potthoff, M. Self – energy – functional approach: Analytical results and the mott – hubbard transition. *Eur. Phys. J. B* **36**, 335 (2003).

[97] Nevidomskyy, A. H., Sénéchal, D. & Tremblay, A. M. S. Convexity of the self – energy functional in the variational cluster approximation. *Phys. Rev. B* **77**, 075105 (2008).

[98] To avoid confusion, we denote as "correlated region" the "physical" one containing interacting sites, bounded by the hoppings V. On the other hand, the "central region" is the one containing the clusters, and is bounded by t_{bic}. (See Fig. 3.1).

[99] Obviously, the uncorrelated leads can be solved exactly without being partitioned into clusters.

[100] Kadanoff, L. P. & Baym, G. *Quantum statistical mechanics: Green's function methods in equilibrium and nonequilibrium problems* (Addison-Wesley, Redwood City, Calif., 1962).

[101] Schwinger, J. *J. Math. Phys.* **2**, 407 (1961).

[102] Keldysh, L. V. *Sov. Phys. JETP* **20**, 1018 (1965).

[103] In the time representation (3.4) they also include convolutions over internal times. However, since we are considering the steady state, Green's functions become diagonal in the frequency representation.

[104] Sénéchal, D., Perez, D. & Pioro-Ladriére, M. The spectral weight of the hubbard model through cluster perturbation theory. *Phys. Rev. Lett.* **84**, 522–525 (2000).

[105] Here, we use a notation to express projection of objects such as G, T, etc., which are matrices in lattice indices and in Keldysh space, onto one of the three regions c, l, or r. More specifically, let m be such a matrix, then m_{AB} refers to a sub-matrix of m in which the left (right) index is restricted to region A (B), with $A, B = c, l$, or r.

[106] For simplicity, we consider all hoppings to be real.

[107] Notice that when the central region coincides with the cluster, $\mathcal{P}G_{CC} = G_{CC}$. In this case the solution of (3.13) is trivially obtained by taking the leads as auxiliary baths.

[108] The $\hat{\tau}_1$ in (3.13) is due to our choice of convention (3.4) for the Keldysh matrix. If one uses the form containing the time- and anti-time-ordered Green's functions in the diagonal, and the greater and lesser in the off-diagonal elements, no $\hat{\tau}_1$ is present in the trace.

[109] Economou, E. N. *Green's Functions in Quantum Physics* (Springer, Heidelberg, 2006).

[110] Pérez-Merchancano, S., Gutiérrez, H. P. & Marques, G. E. Spin transport properties in double-barrier systems with diluted magnetic semiconductor doped layers. *Microelectronics Journal* **39**, 1339 – 1340 (2008). Papers CLACSA XIII, Colombia 2007.

[111] Chioncel, L. *et al.* Electronic correlations in short period $(\text{cras})_n/(\text{gaas})_n$ ferromagnetic heterostructures. *Phys. Rev. B* **83**, 035307 (2011).

[112] Gerbier, F. *et al.* Expansion of a quantum gas released from an optical lattice. *Phys. Rev. Lett.* **101**, 155303 (2008).

[113] Trotzky, S. *et al.* Suppression of the critical temperature for superfluidity near the mott transition. *Nat. Phys.* **6**, 998–1004 (2010).

[114] Kato, Y., Zhou, Q., Kawashima, N. & Trivedi, N. Sharp peaks in the momentum distribution of bosons in optical lattices in the normal state. *Nat Phys* **4**, 617–621 (2008).

[115] Diener, R. B., Zhou, Q., Zhai, H. & Ho, T. Criterion for bosonic superfluidity in an optical lattice. *Phys. Rev. Lett.* **98**, 180404 (2007).

[116] Roth, R. & Burnett, K. Superfluidity and interference pattern of ultracold bosons in optical lattices. *Phys. Rev. A* **67**, 031602 (2003).

[117] Cooper, N. R. & Hadzibabic, Z. Measuring the superfluid fraction of an ultracold atomic gas. *Phys. Rev. Lett.* **104**, 030401 (2010).

[118] Koller, W. & Dupuis, N. Variational cluster perturbation theory for Bose?Hubbard models. *J. Phys.: Condens. Matter* **18**, 9525–9540 (2006).

[119] Potthoff, M. Self-energy-functional approach to systems of correlated electrons. *Eur. Phys. J. B* **32**, 429–436 (2003).

[120] Potthoff, M. Self-energy-functional approach: Analytical results and the Mott-Hubbard transition. *Eur. Phys. J. B* **36**, 335–348 (2003).

[121] Zacher, M. G., Eder, R., Arrigoni, E. & Hanke, W. Evolution of the stripe phase as a function of doping from a theoretical analysis of angle-resolved photoemission data. *Phys. Rev. B* **65**, 045109 (2002).

[122] Fisher, M. E., Barber, M. N. & Jasnow, D. Helicity modulus, superfluidity, and scaling in isotropic systems. *Phys. Rev. A* **8**, 1111 (1973).

[123] Pollock, E. L. & Ceperley, D. M. Path-integral computation of superfluid densities. *Phys. Rev. B* **36**, 8343 (1987).

[124] Prokof'ev, N. V. & Svistunov, B. V. Two definitions of superfluid density. *Phys. Rev. B* **61**, 11282 (2000).

[125] Fisher, M. P. A., Weichman, P. B., Grinstein, G. & Fisher, D. S. Boson localization and the superfluid-insulator transition. *Phys. Rev. B* **40**, 546 (1989).

[126] See App. 4.5.1.

[127] Potthoff, M. Non – perturbative construction of the luttinger – ward functional. *Condens. Matt. Phys.* **9**, 557 (2006).

[128] Here, and below we assume that the relations between conjugate variables are invertible, at least locally, see also App. 4.5.1.

[129] Potthoff, M., Aichhorn, M. & Dahnken, C. Variational cluster approach to correlated electron systems in low dimensions. *Phys. Rev. Lett.* **91**, 206402 (2003).

[130] In VCA [90, 119] the reference system is typically a cluster partition of the original lattice, which can be improved by including bath sites. [132, 133] However, for bosonic systems with $F \neq 0$ and $U < \infty$ the Hilbert space is infinite and the particle number is not conserved. Thus neither a cluster nor a single site can be solved by exact diagonalization. However, a cutoff in the maximum number of bosons can be introduced, which still allows to reach arbitrary accuracy.

[131] The term with G_∞ (see App. 4.5.1) cancels out.

[132] Balzer, M., Hanke, W. & Potthoff, M. Mott transition in one dimension: Benchmarking dynamical cluster approaches. *Phys. Rev. B* **77**, 045133 (2008).

[133] Balzer, M., Hanke, W. & Potthoff, M. Importance of local correlations for the order parameter of high – tc superconductors (2009). ArXiv:0912.1282.

[134] Lieb, E. H., Seiringer, R. & Yngvason, J. Superfluidity in dilute trapped bose gases. *Phys. Rev. B* **66**, 134529 (2002).

[135] Rey, A. M. *et al.* Bogoliubov approach to superfluidity of atoms in an optical lattice **36**, 825–841 (2003).

[136] Poilblanc, D. Twisted boundary conditions in cluster calculations of the optical conductivity in two-dimensional lattice models. *Phys. Rev. B* **44**, 9562 (1991).

[137] Scalapino, D. J., White, S. R. & Zhang, S. C. Insulator, metal, or superconductor: The criteria. *Phys. Rev. B* **47**, 7995 (1993).

[138] Knap, M., Arrigoni, E. & von der Linden, W. Spectral properties of strongly correlated bosons in two-dimensional optical lattices. *Phys. Rev. B* **81**, 024301 (2010).

[139] Albuquerque, A. *et al.* The ALPS project release 1.3: Open-source software for strongly correlated systems. *J. Magn. Magn. Mater.* **310**, 1187–1193 (2007).

[140] Alet, F., Wessel, S. & Troyer, M. Generalized directed loop method for quantum monte carlo simulations. *Phys. Rev. E* **71**, 036706 (2005).

[141] Sandvik, A. & Kurkijärvi, J. *Phys. Rev. B* **43**, 5950 (1991).

[142] Evertz, H. G., Lana, G. & Marcu, M. Cluster algorithm for vertex models. *Phys. Rev. Lett.* **70**, 875 (1993). URL `doi:10.1103/PhysRevLett.70.875`.

[143] Syljuåsen, O. F. & Sandvik, A. W. Quantum monte carlo with directed loops. *Phys. Rev. E* **66**, 046701 (2002).

[144] Rancon, A. & Dupuis, N. Strongly-correlated superfluid near the mott transition. *arXiv:1012.0166* (2010).

[145] Byczuk, K. & Vollhardt, D. Correlated bosons on a lattice: Dynamical mean-field theory for bose-einstein condensed and normal phases. *Phys. Rev. B* **77**, 235106 (2008).

[146] Anders, P., Gull, E., Pollet, L., Troyer, M. & Werner, P. Dynamical mean field solution of the bose – hubbard model. *Phys. Rev. Lett.* **105**, 096402 (2010).

[147] Tomadin, A. & Fazio, R. Many-body phenomena in QED-cavity arrays. *J. Opt. Soc. Am. B* **27**, A130–A136 (2010).

[148] Barnett, R., Petrov, D., Lukin, M. & Demler, E. Quantum magnetism with multicomponent dipolar molecules in an optical lattice. *Phys. Rev. Lett.* **96**, 190401 (2006).

[149] Micheli, A., Brennen, G. K. & Zoller, P. A toolbox for lattice-spin models with polar molecules. *Nat. Phys.* **2**, 341–347 (2006).

[150] Aichhorn, M., Evertz, H. G., von der Linden, W. & Potthoff, M. Charge ordering in extended hubbard models: Variational cluster approach. *Phys. Rev. B* **70**, 235107 (2004).

[151] Kollath, C., Schollwöck, U., von Delft, J. & Zwerger, W. Spatial correlations of trapped one-dimensional bosons in an optical lattice. *Phys. Rev. A* **69**, 031601 (2004).

[152] Luttinger, J. M. & Ward, J. C. Ground – state energy of a many – fermion system II. *Phys. Rev.* **118**, 1417–1427 (1960).

[153] Schulman, L. S. *Techniques and Applications of Path Integration* (Wiley, New York, 1981).

[154] Arrigoni, E., Castellani, C., Grilli, M., Raimondi, R. & Strinati, G. C. Functional–integral formulation of the slave–boson approach: Beyond the mean–field treatment with the correct continuum limit. *Phys. Rep.* **241**, 291–371 (1994).

[155] Arrigoni, E. & Strinati, G. C. Beyond the gutzwiller approximation in the slave–boson approach: Inclusion of fluctuations with the correct continuum limit of the functional integral. *Phys. Rev. Lett.* **71**, 3178–3181 (1993).

[156] Arrigoni, E. & Strinati, G. C. Correct continuum limit of the functional–integral representation for the four–slave–boson approach to the hubbard model: Paramagnetic phase. *Phys. Rev. B* **52**, 2428–2462 (1995).